

Using GEDI Data to Evaluate the Impact of the Australian 2019-2020 Fire Season on the
Structure and Biomass of Gondwana Rainforests

A Thesis submitted in partial fulfillment of the requirements for the degree of Master of
Science at George Mason University

by

Colin G. Flynn
Bachelor's Degree
George Mason University, 2019
Associate's Degree
Northern Virginia Community College, 2017

Director: Konrad Wessels, Associate Professor
Department of Geography and Geoinformation Science

Fall Semester 2022
George Mason University
Fairfax, VA

Copyright 2022 Colin G. Flynn
All Rights Reserved

DEDICATION

I dedicate this work to . . .

ACKNOWLEDGEMENTS

I wish to thank my advisor, Dr. Konrad Wessels, for his guidance and support throughout this process; his knowledge has been invaluable. I also want to thank the members of my committee for their invaluable input: Dr. Paul Houser and Dr. Edward Oughton. I want to thank Xiaoxuan Li for all his help with processing GEDI data, and Dr. John Armston for his advice for his advice on GEDI metrics. Additionally, I would like to thank my wife Nicole, for her patience and support throughout my time in graduate school.

TABLE OF CONTENTS

	Page
List of Tables	vi
List of Figures	vii
List of Equations	ix
List of Abbreviations and/or Symbols	x
Abstract	xii
Chapter One	1
1. Introduction	1
2. Literature Review	8
3. Research Questions	15
4. Materials and Methods	16
4.1 Study Area	17
4.2 MODIS Burned Area	20
4.3 Landsat 8 spectral indices	21
4.4 GEDI Data	22
4.4.1 Filtering GEDI data for best results	27
4.5 Grid Cells	28
5. Results	29
5.1 GEDI vegetation metrics	32
5.2 Satellite indices	Error! Bookmark not defined.
5.3 Uncertainty	Error! Bookmark not defined.
6. Discussion and Conclusion	42
Appendix	51
References	67

LIST OF TABLES

Table	Page
Table 1 Satellite Systems and the bands used in this study	21
Table 2 GEDI PAVD vertical profile height bins.....	26
Table 3 Summary Statistics from SA1 and SA2.....	39
Table 4 Correlation coefficients for each of the studied variables in SA1	40

LIST OF FIGURES

Figure	Page
Figure 1 Study areas overview map showing Study Area 1 (SA1) in red and Study Area 2 (SA2), the control area, in green with an inset showing where in Australia the study areas are located	4
Figure 2 Study Area 1 (SA1) overview map with grid cells, pre-fire, and post-fire GEDI points over a digital elevation model with hillshade	19
Figure 3 Study Area 2 (SA2) overview map with grid cells, pre-fire, and post-fire GEDI points over a digital elevation model with hillshade	20
Figure 4 Illustration of the ground sampling pattern that GEDI uses. The dashed lines represent the result of dithering each beam to produce 8 different ground tracks of data. There is a 60 meter distance between GEDI footprints along track and a 600 meter distance between GEDI footprints across track.	24
Figure 5 Boxplot of average Normalized Burn Ratio (NBR), on the left, and Normalized Difference Vegetation (NDVI), on the right, in SA1 with green representing pre-fire values and brown representing post-fire values.....	31
Figure 6 Percent change in each GEDI Relative Height (RH) metric in Study Area 1	32
Figure 7 Boxplot of GEDI Relative Height (RH) metrics in Study Area 1	33
Figure 8 Boxplot of GEDI Relative Height (RH) metrics in the control area	34
Figure 9 Comparison of the percent change in GEDI observed Plant Area Index (PAI), Foliage Height Diversity (FHD) and Canopy Cover Fraction (CCF) in SA1 (shown in red) and in SA2, the control area (shown in green)	35
Figure 10 Percent change in GEDI Plant Area Volume Density (PAVD) by vertical profile height bin in Study Area 1 where each height bin has a vertical resolution of 5 meters and the bins range from 0-5 meters to 35-40 meters.....	37
Figure 11 Boxplot of GEDI Plant area volume density (PAVD) showing pre-fire (green) and post-fire (brown) by vertical profile height bin in Study Area 1. Blue lines in boxes indicate the median value.....	38
Figure 12 Boxplot of average Normalized Burn Ratio (NBR), on the left, and Normalized Difference Vegetation (NDVI), on the right, in SA2 with green representing pre-fire values and brown representing post-fire values.....	49
Figure 13 Percent change in each GEDI Relative Height (RH) metric in Study Area 2..	50
Figure 14 Percent change in GEDI Plant Area Volume Density (PAVD) by vertical profile height bin in Study Area 2 where each height bin has a vertical resolution of 5 meters and the bins range from 0-5 meters to 35-40 meters.....	51
Figure 15 Boxplot of GEDI Plant area volume density (PAVD) showing pre-fire (green) and post-fire (brown) by vertical profile height bin in Study Area 1. Blue lines in boxes indicate the median value.....	52
Figure 16 Plant Area Index (PAI) values from SA1	53
Figure 17 Foliage Height Diversity (FHD) values from SA1.....	54
Figure 18 Canopy Cover Fraction (CCF) values from SA1	55

Figure 19 Plant Area Index (PAI) values from SA2.....	56
Figure 20 Foliage Height Diversity (FHD) values from SA2.....	57
Figure 21 Canopy Cover Fraction (CCF) values from SA2	58
Figure 22 Plant Area Index (PAI) scatterplot, SA1	59
Figure 23 Foliage Height Diversity (FHD) scatterplot, SA1	60
Figure 24 Canopy Cover Fraction (CCF) scatterplot, SA1	61
Figure 25 Plant Area Index (PAI) scatterplot, SA2	62
Figure 26 Foliage Height Diversity (FHD) scatterplot, SA2.....	63
Figure 27 Canopy Cover Fraction (CCF) scatterplot, SA2	64

LIST OF EQUATIONS

Equation	Page
Equation 1 Normalized Burn Ratio (NBR) calculation	22
Equation 2 Normalized Difference Vegetation Index (NDVI) calculation	22

LIST OF ABBREVIATIONS

Above Ground Biomass Density	AGBD
Airborne Laser Scanning	ALS
Algorithm Theoretical Basis Document	ATBD
Atmospheric Dynamics Mission.....	ADM-Aeolus
Burn Area Index.....	BAI
Canopy Cover Fraction.....	CCF
Cloud-Aerosol Lidar and Infrared Pathfinder Satellite Observations	CALIPSO
Cloud-Aerosol Transport System	CATS
Composite Burn Index	CBI
Delta Leaf Area Index.....	dLAI
Diameter at Breast Height.....	DBH
Digital Elevation Model.....	DEM
Differenced Normalized Burn Ratio.....	dNBR
Differenced Normalized Difference Vegetation Index.....	dNDVI
Differenced Normalized Difference Water Index.....	dNDWI
Earth Ventures Instrument	EVI
Food and Agricultural Organization	FAO
Fire Radiative Power	FRP
Foliage Height Diversity	FHD
Global Ecosystem and Dynamics Investigation	GEDI
Hectares	ha
Ice Cloud and Land Elevation Satellite	ICESat
Land Processes Distributed Active Archive Center.....	LPDAAC
Leaf Area Index	LAI
Light Detection and Ranging.....	Lidar
LiDAR Height Diversity Index.....	LHDI
LiDAR Height Evenness Index	LHEI
Mean Absolute Error.....	MAE
Megagrams per Hectare	Mg/Ha
Moderate Resolution Imaging Spectroradiometer	MODIS
Monitoring Trends in Burn Severity.....	MTBS
National Aeronautics and Space Administration.....	NASA
National Agriculture Imagery Program	NAIP
Near-infrared.....	NIR
Normalized Burn Ratio.....	NBR
Normalized Difference Vegetation Index.....	NDVI
Oak Ridge National Laboratory Distributed Active Archive Center.....	ORNLDAAC
Profile Area Change.....	PAC
Plant Area Index	PAI
Plant Area Volume Density	PAVD

Random Forest	RF
Relative differenced Normalized Burn Ratio	RdNBR
Relative Height	RH
Root Mean Squared Error	RMSE
Study Area 1	SA1
Study Area 2	SA2
Short-wave Infrared	SWIR
Standard Deviation.....	STD
Subtropical Humid Forest	SCf
Support Vector Machine	SVM
Temperate Mountain System	TeM
Top of Canopy	TOC
United Nations	UN
UN Educational, Scientific and Cultural Organization	UNESCO

ABSTRACT

USING GEDI DATA TO EVALUATE THE IMPACT OF THE AUSTRALIAN 2019-2020 FIRE SEASON ON THE STRUCTURE AND BIOMASS OF GONDWANA RAINFORESTS

Colin G. Flynn, M.S.

George Mason University, 2022

Thesis Director: Dr. Konrad Wessels

Wildfires are increasing globally in their intensity, frequency, and range. A unique yet globally significant example is the devastating eastern Australia 2019-2020 fire season, which resulted in an unprecedented burnt forest area with > 21% of Australia's temperate forests affected, and, in an unprecedented event, over 50% of Gondwana Rainforests in Australia were impacted. Currently, optical satellite imagery is used to detect active fires and assess burnt area, as well as impact. Assessing the impacts of fires solely through these techniques lacks information on vegetation structural changes, especially subcanopy changes. Lidar (light detection and ranging) can be used to evaluate the impacts of fire on vegetation structure more comprehensively. This study uses full waveform lidar data from NASA's Global Ecosystem Dynamics Investigation (GEDI) to study the Gondwana Rainforests of Willi Willi National Park and Werrikimbe National Park, in New South Wales, Australia. GEDI footprints were filtered to remove

those incident upon steep slopes ($>25^\circ$) and collected more than 9 months before and after the MODIS recorded burn date. GEDI footprint level canopy structure measurements (Level 2A and 2B data products) were aggregated into 5 km² grid cells across the study sites and showed an average decrease of 19% in Plant Area Index, and a 15% decrease in Canopy Cover Fraction. Vertical profiles of Plant Area Volume Density (PAVD) grouped into 5 meter vertical profile height bins showed an average decrease of -15.6% (STD = 8.1) for bins from 0-5 meters to 35-40 meters, with the largest decrease of -27.63% occurring in the 10-15 meter vertical profile height bin. GEDI relative height (RH) metrics were lower post fire: RH50 decreased by average of 12.7%, RH75 by 5.1%, and RH90, RH95, RH98, and RH100 all by $<1\%$. GEDI footprint level aboveground biomass density (Level 4A product) showed a -1.5% decrease, correlating closely with percent change in RH75 and the 20-25 meter PAVD vertical profile height bin. The PAVD metric change therefore captured the impact of the fire more effectively than RH metrics, which showed limited change. Consequently, the footprint-level GEDI biomass which is largely derived from RH metrics show minor changes after the fire. These results indicate that GEDI was uniquely positioned to directly quantify the effects of vegetation disturbance on vertical canopy structure. The structural damage resulting from these fires ranged from entire stand-replacing disturbance to primarily crown or understory fires. We discuss the potential implications of these findings to understand the impact of fire severity and post-fire recovery on carbon stocks at regional scales.

CHAPTER ONE

All material in the document must adhere to [University Formatting Guidelines](#).

For questions and further information, please contact the UDTS Coordinator:

udts@gmu.edu.

1. INTRODUCTION

Wildfires are large ecological disturbances that can have varying impacts in different ecosystems. Recently, intense and widespread fires have been occurring across the world, including in the United States, Brazil, Russia, Australia, and other countries (Keeley & Syphard, 2021; Assis et al., 2020; Kirillina et al., 2020; Bowman et al., 2021). The consequences of these fires are far-reaching, affecting ecosystems, wildlife, economies, and the climate. Research has demonstrated links between climate change and increased risk of wildfires in Amazonia, Southern Europe, Scandinavia, Western United States, Canada, Siberia, and Australia (Jones et al., 2020). Increases in both the intensity and frequency of fires have been linked to climate change, and this trend is expected to continue (Jolly et al., 2015). In 2008, Garnaut correctly predicted that climate change would exacerbate fires in Australia (Garnaut, 2008). Appropriately, the 21st century has been dubbed “the age of the megafire” by mainstream media.

Australia’s 2019-2020 summer and fire season came with record breaking megafires across the continent, and consequently it is now commonly referred to as the

“Black Summer” (Scott Morrison, 2020). For megafires such as this to occur on a landscape-scale, four specific conditions must first be met: (1) presence of spatially continuous fuel, (2) the fuel must be dry enough to burn, (3) presence of an ignition source, (4) weather conditions conducive to the spread of fire (Nolan et al., 2020). The largest impedance to large fires occurring in Australia is the second condition, as many of the abundant fuel sources are infrequently dry enough, while the other conditions are commonly met. Prior to the start of the fires in 2019, eastern Australia was experiencing an extreme drought, with New South Wales experiencing record low rainfall in addition to above average temperatures (Nolan et al., 2020). This drought led the biomass in Australian forests to dry out significantly. The Black Summer consumed 5.68 million ha of land in New South Wales, alone (Davey & Sarre, 2020). Recent research claims that climate change made these fires 30% more likely to occur (van Oldenborgh et al., 2021). Across Australia, the 2019-2020 bushfires claimed a combined total of 10.2 million ha (Davey & Sarre, 2020).

In comparison, the 2018 fire season, the most destructive wildfire season in California in recorded history, impacted 675,825 ha, which is 1/15 of the area burned in the 2019-2020 Australian fire season (California Government, 2019). The Black Summer burned over five times the amount of land burned in the Amazon Rainforest in 2019 (Ward et al., 2020). New research from the National Oceanic and Atmospheric Administration (NOAA) states that nearly 1 million metric tons of carbon were released by these fires (Yu et al., 2021). According to the World Wildlife Fund, almost 3 billion animals were killed or displaced by the Black Summer fires (*New WWF Report*, 2020).

Most of the burned area was across regions and ecosystems that are prone to frequent burns and are considered to be fire resilient, such environments include the eucalypt forests. In addition to the spatial extent and temporal duration of the 2019-2020 fire season, it was furthermore unique in that certain Australian ecosystems that do not typically burn during fire seasons, experienced many active fires. The Gondwana Rainforests are one such noteworthy ecosystem. The Gondwana Rainforests are a UNESCO World Heritage Site made up of a conglomeration of over 50 nationally protected sites. Together, these make up the world's largest stands of existing subtropical rainforests and Antarctic Beech cool temperate rainforests. During the Black Summer, over 50% of the Gondwana Rainforests were impacted by fires, an unprecedented amount (Kooyman et al., 2020). Anticipating that climatic trends will continue to increase the propensity for fires to occur in such environments, it is important to develop more knowledge around how these historic forests are impacted.

This research focuses on evaluating the impacts of forest fires in Gondwana Rainforests through two separate study areas. Study area 1 (SA1) is composed of Werrikimbe National Park and Willi Willi National Park. These two national parks are spatially contiguous and are treated as one site for this study. Separately, Barrington Tops National Park is study area 2 (SA2), which serves as a control, as it did not experience significant burning during the Black Summer. Both study areas are on the east coast of New South Wales, Australia (Figure 1).

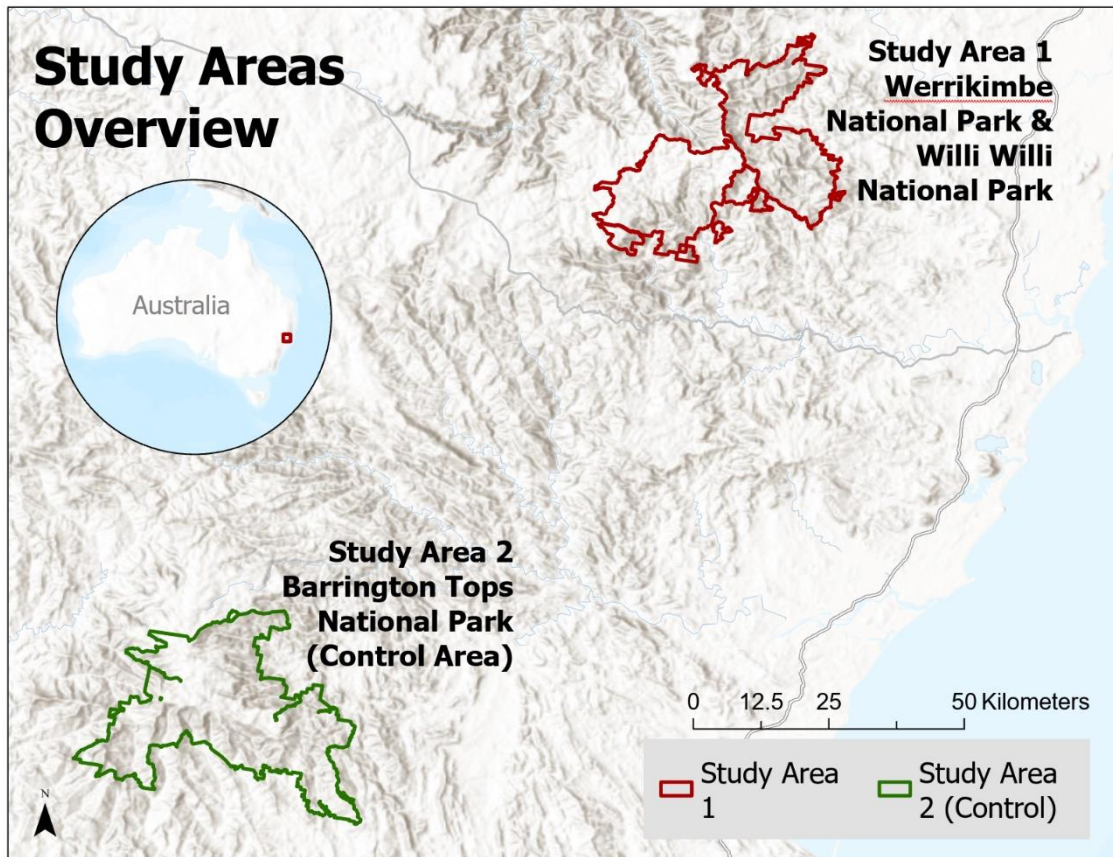


Figure 1 Study areas overview map showing Study Area 1 (SA1) in red and Study Area 2 (SA2), the control area, in green with an inset showing where in Australia the study areas are located

At present, fires are routinely detected and evaluated using passive satellite remote sensing (Wooster et al., 2021). Passive remote sensing systems record the response of the radiation on the Earth’s surface that is either reflected or emitted (Camarretta et al., 2020). Active fire remote sensing assesses when and where fires occur as well as their fire radiative power, or FRP (Wooster et al., 2021), fire severity (Keeley, 2009), and fire emissions (Kaufman et al., 1990). Satellite imagery collected before and after a fire event are used in conjunction to estimate the impacts of the fire on vegetation through spectral changes. While satellite imagery is the most effective way to detect

active fires (Boer et al., 2008), other, more robust techniques to assess the post-fire impacts on vegetation must be investigated further. Conventional methods of evaluating fire severity with multispectral satellite imagery utilize both low earth orbit and geostationary satellites (van Gerrevink & Veraverbeke, 2021). Commonly used for these purposes, passive remote sensing systems, such as Landsat, Sentinel, Worldview, MODIS, and others, are incapable of providing any information in regards to fire-induced changes in the vertical structure of vegetation, with an exception for observable stand-replacing fire events.

Fire severity is a way of measuring the physical changes in the environment caused by fire. Fire severity evaluations can be conducted manually with indices based on field observations, such as the composite burn index (CBI). However, such indices that are reliant on field work are only able to sample plots of large fires (De Santis & Chuvieco, 2009). Alternatively, satellite imagery and spectral indices, which can provide wall-to-wall coverage of a fire area, are frequently used to categorize fire severity. Different spectral indices, such as the burn area index (BAI), normalized burn ratio (NBR) and delta normalized burn ratio (dNBR), delta normalized difference vegetation index (dNDVI), and delta normalized difference water index (dNDWI) are frequently used (Tran et al., 2018). While these are the most widely used methods for evaluating fire severity through remote sensing, it has been shown that these are not consistently sensitive to fire severity (Roy et al., 2006). The comparison between ground-based CBI observations and dNBR by Cocke et al. demonstrates the potential for disparities between multispectral satellite derived burn severity assessments and impacts on forest structure

(Cocke et al., 2005). As shown by Tran et al., study site characteristics impact how well burn indices perform and might lead one to perform better than others (2018).

Evaluations of wildfires utilizing these passive optical methods rely on how severely top of canopy (TOC) was impacted by the fire. Changes in vegetation structure may not be accurately represented in this manner. Consequently, research and development of novel metrics for assessing wildfire impact on vegetation structure, inclusive of changes in the midstory and understory, is needed to augment current, passive optical approaches. The integration of 3-dimensional information on the physical structure of vegetation will provide a more comprehensive depiction of how vegetation responds to and is impacted by fires at varying levels of severity. Lidar is an active remote sensing system, wherein sensor emits laser pulses and records the energy as it returns, distributed over time, yielding a waveform. Geospatial lidar data is recorded and analyzed using different methods, two main branches being discrete return lidar point clouds, and full waveform lidar data. Discrete return airborne lidar, also referred to as airborne laser scanning (ALS) is widely used to produce high resolution digital elevation models (DEMs), which are useful for things such as flood plain mapping, agriculture, and archaeology. In 2000, Dubayah and Drake embraced lidar as a “breakthrough technology with many forestry applications (Dubayah & Drake, 2000). Appropriately, lidar data has been widely employed in this area. Lidar can be used to estimate biomass (Duncanson et al., 2020; Stoval et al., 2018; J Wu, et al., 2009), changes in forest structure (Davison et al., 2020; Zhao et al., 2011; Wang & Fang, 2020; Boucher et al., 2020), and even distinguish vegetation types (Marselis, et al., 2018). ALS data has also been used

successfully to map fire severity (Hu et al., 2019), but pre- and post-fire ALS acquisitions are surprisingly rare, thus limiting the application of lidar to this research topic.

Waveform lidar has the benefit of modeling 3-dimensional vegetation structure (Camarretta et al., 2020). Vegetation structural metrics can be accurately derived from such data. Geospatial lidar is primarily collected with sensors on piloted aircraft or drones. Additionally, there have been several space-based satellites with lidar instruments, including NASA's Ice Cloud and Land Elevation Satellite (ICESat) and ICESat-2, the Cloud-Aerosol Transport System (CATS), the Cloud-Aerosol Lidar and Infrared Pathfinder Satellite Observations (CALIPSO), the Atmospheric Dynamics Mission (ADM-Aeolus), and the Global Ecosystem Dynamics Investigation (GEDI) (Fouladinejad et al., 2019). The structural metrics derived from the GEDI LiDAR waveform is very well suited to capturing vertical forest structure, but at the time of writing there has been no studies published to evaluate the effectiveness of these GEDI metrics in characterizing the impacts of wildfire on forest structure.

This study proposes the use of full waveform lidar data from the space-borne GEDI mission and derived metrics to evaluate changes in vegetation structure caused by wildfire (Dubayah et al., 2020). Observed changes in GEDI vegetation structural metrics will be evaluated and their relationship to multispectral burn indices examined using two Gondwana Rainforests study sites in New South Wales, Australia during the 2019-2020 fire season.

2. LITERATURE REVIEW

Many examples of successful applications of different burn indices can be found in the literature. Different platforms and sensors can be used to generate them. Wildfires in Australia are being heavily researched by the Australian government and the academic community. The causes and impacts of such fires as well as the role that climate change plays are all being investigated. Lidar data from GEDI has been applied to numerous applications in the brief time span since NASA first began releasing data from the sampling mission. Validation studies have shown the potential for GEDI data to be used reliably (Hancock et al., 2019; Liu et al., 2021; Rishmawi et al., 2021). However, at the time of authoring this paper, nothing has been published on the use of GEDI data to evaluate structural changes in vegetation following a fire event. Separately from GEDI, ALS data can be used as a method for evaluating the impacts of fires, but it is often limited to a single temporal collection rather than using pre-fire and post-fire data as is used for passive remote sensing methods.

In 1996, White et al. researched burn severity with Landsat data in Glacier National Park, United States. Their research helped develop a better understanding of where and how regrowth occurs following fires and found satellite-based techniques for evaluating forest fires to be useful (White et al., 1996). However, as with many burn severity studies the structural impacts of the fire were not evaluated.

Cocke et al. showed that burn severity can be mapping with satellite data through their case study in the mixed conifer forests in the Coconino National Forest in Arizona, United States (Cocke et al., 2005). They compared dNBR values to composite burn index

(CBI) values. CBI is a method of evaluating fire severity with ground-based observations. They found that tree density, basal area, snag density and fine fuel accumulation were all associated with the severity level from the dNBR. Their conclusions noted that dNBR was not accurate for mapping perimeters but did identify areas that were severely burned.

Boer and his team mapped burn severity in Australia in 2008 using dNBR, NDVI, and a delta Leaf Area Index (dLAI). They found LAI to be a large contributor to NBR values. Boer concluded that LAI can be used to effectively map burn severity in Eucalypt forests (Boer et al., 2008). They also contend that this method of evaluation is preferable to more standard approaches, such as the DNBR, because it is more easily interpreted within the context of ecological forest management.

Tran et al. (2018) comprehensively reviewed 10 different burn indices in Australian temperate forests. Their study included 13 different forest types and helped highlight that different burn indices perform well in certain forest types and poorly in others. This shows that any single burn index should not be used across the board as a standard. They found that dNBR performed the best for open forests and woodlands, while dNDVI performed best in open forests that had mixed fire responses, and dNDWI was the most accurate in closed forests. This study used cross-validation as a means of quantifying the accuracies of the indices and did not consider any field data or means of assessing changes to forest structure. They also highlighted that rainforest environments, such as the Gondwana Rainforests studied here, were not particularly sensitive to any of the metrics they tested (Tran et al., 2018). This reiterates the need for the development of new methods to evaluate the impacts of fires on forestry.

Miller and Thode proposed using a relative version of the dNBR to quantify burn severity. They acknowledged that absolute change, as most burn indices measure, can be inappropriate for the assessment of ecological implications (Miller & Thode, 2007). This research pointed out that current approaches can result in misclassifications due to different vegetation types being evaluated with the same method.

A recent study on burn severity in North Patagonian forests sought to establish a relationship between spectral burn indices and field measurements, noting that in such environments “studies aimed at the field validation of spectral indices of burn severity are scarce” (Franco et al., 2020). They used a modified composite burn index (mCBI) as a field-based measurement of fire severity and found dNBR and dNDVI to be the most accurate spectral indices in comparison. Accuracies here were higher in instances of severe burns, while both user and producer accuracies reached 50% for moderate severity (Franco et al., 2020).

The Monitoring Trends in Burn Severity (MTBS) program, a multiagency program in the United States, started in 2006 with the goal of consistently mapping fire perimeters and burn severity (Gao et al., 2020). A 2015 review by Kolden, et al. addressed limitations in the MTBS data products. They found the data to be “of limited use to research due to a lack of both consistency in developing class thresholds and empirical relationships with ecological metrics” (Kolden et al., 2015).

Reilly et al. studied impacts of wildfires on fuel load and forest structure in Mediterranean ecosystems in California by using multispectral imagery and structure from motion from unoccupied aerial systems. They compared their canopy structure and

terrain height to pre-fire ALS data and found that their methods accurately mapped the upper canopy but failed to resolve mid and below canopy structure. Their post-fire assessment showed that even two years after the fire event, there were significant differences in bulk canopy height and NDVI. They suggest the use of UAS to monitor forests and provide post-fire assessment data (Reilly et al., 2021). While this study used lidar data, they were not able to use any from after the fire and, as they pointed out, could not resolve canopy changes below the upper canopy. Full waveform data as generated by GEDI is designed specifically to offer more detailed information about vegetation structure throughout the entire canopy and understory (Dubayah et al., 2020).

Gelabert et al. used low point density (<4 points per m²) ALS data to analyze differences in structural diversity in Aleppo pine tree forests that had been affected by wildfires in the Mediterranean Basin. From the ALS data, they derived the LiDAR Height Diversity Index (LHDI), LiDAR Height Evenness Index (LHEI), the vertical and horizontal continuity of vegetation and topographic metrics. The authors used these metrics with the *k*-nearest neighbors (*k*-NN) algorithm, support vector machine (SVM) and random forest (RF) models to map burned and unburned areas and differentiate fire occurrence dates. Their results showed lower LHDI and LHEI values for recent fires and higher values for older fires (>20 years) due to growth of trees and shrubs. Their RF method produced the most accurate burn mapping with an accuracy of 89.64%, and the SVM model was best able to structural differences between fires, achieving a 68.79% accuracy (Gelabert et al., 2020).

Fires in Mediterranean pine forests were also researched by Montealegre et al. (2014) in a study that used CBI field estimations with ALS data to map fire severity with logistic regression modeling. They found the most important regression variables to be the canopy relief ratio and the percentage of all returns above one meter height, the results achieved up to 85.5% accuracy (Montealegre et al., 2014).

In 2012, Magnussen and Wulder published a study using a single collection of ALS data in Canada to derive a least-squares polynomial (LSPOL) relationship between heights of presumed post-fire recovered canopies and the number of years since fire. They used ALS data and Landsat imagery to derive fire boundaries, the results of which were used to denote lidar points being inside or outside of a fire. The authors used the LSPOL to estimate post-fire aboveground biomass (Magnussen & Wulder, 2012).

A 2019 study proposed a novel method for quantifying fire-induced forest structural changes based on profile area change (PAC). Their method using pre-fire and post-fire lidar data to measure the difference in profile area was tested in the Sierra Nevada, California for a 2013 fire. They found a correlation between PAC and field measurements (basal area and LAI), with an R^2 value of at least 0.67. PAC correlated much more closely than other tested lidar metrics: canopy cover and tree height metrics ($R^2 \leq 0.43$). Additionally, they found that Landsat based RdNBR (relative differenced normalized burn ratio) correlated even more poorly with field measurements ($R^2 \leq 0.26$). The authors also conclude that PAC can be used to determine where canopy loss and subcanopy loss occurs (Hu et al., 2019).

Bishop et al. tested different combinations of lidar data and imagery for post-fire assessments of wildfire impacts. Their study used 47 plots of 0.08 ha; they estimated percent mortality among trees with DBH (diameter at breast height) values over 25.4 cm. Plots with less than 25% mortality were categorized as low, plots categorized as moderate had mortality between 25-50%, and anything over 50% was considered high mortality. Their model which only used NDVI, derived from NAIP (National Agriculture Imagery Program) imagery, was found to be 74% accurate; their model which combined NDVI and post-fire lidar was 85% accurate; finally, their model using NDVI and differenced (pre-fire and post-fire) lidar was 83% accurate. They concluded that the moderate improvement in accuracy with the addition of post-fire lidar data might not justify the expense of collecting it instead of solely using imagery (Bishop et al., 2014).

Although not dealing with wildfires, Peter Scarth and his coauthors investigated the use of ALOS PALSAR radar data, ICESat/GLAS lidar data, and Landsat multispectral data to derive structural classifications for Australian Vegetation with data collected between 2003 and 2009. The waveform lidar based vegetation metrics provided by the sampling missions of ICESat and Glas were extrapolated across Australia using L-band synthetic aperture radar data from ALOS and foliage projective cover from Landsat. Height accuracy issues with ICESat led to reduced accuracy and the study found that results were less reliable in sparsely vegetated areas such as savannas (Scarth et al., 2019).

Prior to the launch of the GEDI mission, many researchers simulated GEDI data from discrete return lidar point clouds collected via airborne laser scanning (ALS). Such

research established that GEDI data could be compared to discrete return lidar data that was used to simulate full waveform lidar like that produced by GEDI. Research shows that ALS data with at least 4 points per square meter can be used to accurately identify the ground within 1 meter. GEDI being a sampling mission, no two paths of data will directly overlap and allow for tree level comparisons (Boucher et al., 2020). Boucher and coauthors studied changes to forest structure with simulated GEDI data, showing the impacts that Hemlock Woolly Adelgid infestations can have in forests. Change metrics were computed between waveforms simulated from lidar collected at different dates. Plant area index (PAI) and relative height (RH) metrics were used in this study. They found a strong correlation between infested trees and reduced PAI and RH metrics (Boucher et al., 2020).

Research by Potapov et al. (2021) used GEDI data and Landsat data to create a global forest canopy height map / data product for 2019 at a 30 meter spatial resolution. Local ALS lidar data was used to determine which RH metric was used for canopy height in different regions. Their regression tree machine learning model predicted a forest height value based on multispectral data from Landsat based on training data from GEDI RH metrics. Comparing their results to available GEDI data (not used for training the model) and ALS data yielded values R^2 values of 0.62 and 0.61 with RMSE (root mean squared error) values of 6.6 meters and 9.07 meters and MAE (mean absolute error) values of 4.45 meters and 6.36 meters, respectively (Potapov et al., 2021).

Recent research using 119 study sites in south-eastern Australia, demonstrated the impacts that logging and wildfires can have on the height and density of forest

vegetation. They used portable weather stations to monitor and collect data on air temperature, relative humidity, vapour pressure deficit and windspeed. As time since loggings increased, the relative humidity and fuel moisture increased. These changes were accompanied by decreasing windspeeds, temperature, vapour pressure deficit and lower Forest Fire Danger Index values (Wilson et al., 2022). Overall, their research showed that changes in vegetation structure attributed to logging, or, to a lesser extent, wildfires, increased the risk of fire (Wilson et al., 2022). In the context of this research, a better understanding of structural changes to vegetation structure is of heightened importance as it influences the risk for more wildfires.

There are limited studies relating widely used burn indices to changes in vegetation structure due to wildfire over large areas. Pre-fire and post-fire high quality lidar data for a study site are infrequently available, limiting the number of opportunities to study how lidar data evaluates changes to forest structure. The timing of GEDI's presence collecting data from the ISS allows for a novel lidar based derivation of changes in forest structure metrics and for a comparison to frequently used satellite derived spectral indices.

3. RESEARCH QUESTIONS

This research aims to answer 4 research questions:

1. How do observed changes in vegetation structure relate to spectral indices of burn severity? Changes in GEDI metrics might be correlated with commonly derived satellite indices that use changes in spectral signatures to derive and quantify burn severity. GEDI could capture changes in a manner unable to be captured with passive

remote sensing techniques. GEDI metrics related to the understory are essentially observing a different target than the TOC measurements recorded by optical imagery.

2. What differences can be observed in GEDI metrics between pre-fire and post-fire footprints? GEDI RH metrics, vertical profile metrics, and canopy cover estimates have never (to our best awareness) been used to evaluate fire-induced changes. It is unknown how each different GEDI metric will measure the changes.

3. Which of the GEDI metrics offer the most insight into fire-induced changes in vegetation structure? Certain GEDI metrics might respond more directly to changes in vegetation structure depending on the vertical location in the forest that the fire occurred. Fires do not always impact the forest all the way up to the canopy; depending on the conditions and availability of fuel, fires can burn more intensely in the understory or amongst shrubs.

4. What changes do GEDI L4A above ground biomass density estimations show, and can they be used to derive carbon emissions estimations? Accurate biomass estimations allow for direct derivations of carbon emissions. GEDI's primary science goal is the creation of accurate above ground biomass density (AGBD) estimates (Duncanson et al., 2022), this research offers a unique perspective on how those data reflect fire-induced changes in forest structure.

4. MATERIALS AND METHODS

The methods used in this study are broken down into five components. First, the MODIS burned area product is used to identify when and where fires took place surrounding the identified study area of the Gondwana Rainforests located in New South

Wales, Australia. Second, using the burn dates identified, appropriate Landsat 8 data is downloaded and used to calculate the burn indices used in this study. Next, L2A, L2B, and L4A GEDI data are downloaded and separated into pre-fire and post-fire datasets for each study area. The GEDI data is then filtered based on quality flags, slope, and to include only records from within nine months pre and post burn. 5 km² grid cells are created for each study area and only those with a minimum of 50 GEDI footprints for both before and after are retained for processing. The remaining data are then used for change analyses.

4.1 Study Area

This study uses Willi Willi National Park and Werrikimbe National Park as a conjoined primary study area, referred to as Study Area 1 (SA1). The entirety of Willi Willi National Park is classified as temperate mountain system (TeM) according to the Food and Agricultural Organization (FAO) of the UN, while Werrikimbe National Park is mostly TeM and partly subtropical humid forest (SCf). 88% and 96% of the land in Willi Willi National Park and Werrikimbe National Park, respectively, were affected by fire during the 2019-2020 fire season (Commonwealth of Australia, Department of Agriculture, Water and the Environment, 2020). The average annual rainfalls for the national parks in SA1 are between 1000-1500 mm per year (Australian Government Bureau of Meteorology, n.d.). Average annual rainfall in Barrington Tops National Park (SA2) ranges between 1000 and 2000 mm (*Barrington Tops National Park, Mount Royal National Park and Barrington Tops State Conservation Area Plan of Management*, 2022). Werrikimbe National Park has an average summer temperature between 16°C and

29°C, while winter temperatures average between 5°C and 20°C (*Werrikimbe National Park / Visitor Info*, n.d.). Willi Willi National Park has less variation in its average temperatures, with the average for summer being between 26°C and 28°C and winter between 16°C and 20°C (*Willi Willi National Park / Visitor Info*, n.d.). Willi Willi National Park, and other areas affected by the fires, hold cultural significance to indigenous tribes such as the Dunghutti Aboriginals (Office of Environment & Heritage, 2011). 23 of the plants native to Willi Willi National Park are considered threatened (Office of Environment & Heritage, 2011). According to the New South Wales National Parks and Wildlife Service, Werrikimbe National Park is home to more than 200 animal species and roughly 1000 different plant species, of which almost 30 are rare or threatened (*Werrikimbe National Park / Learn More*, n.d.).

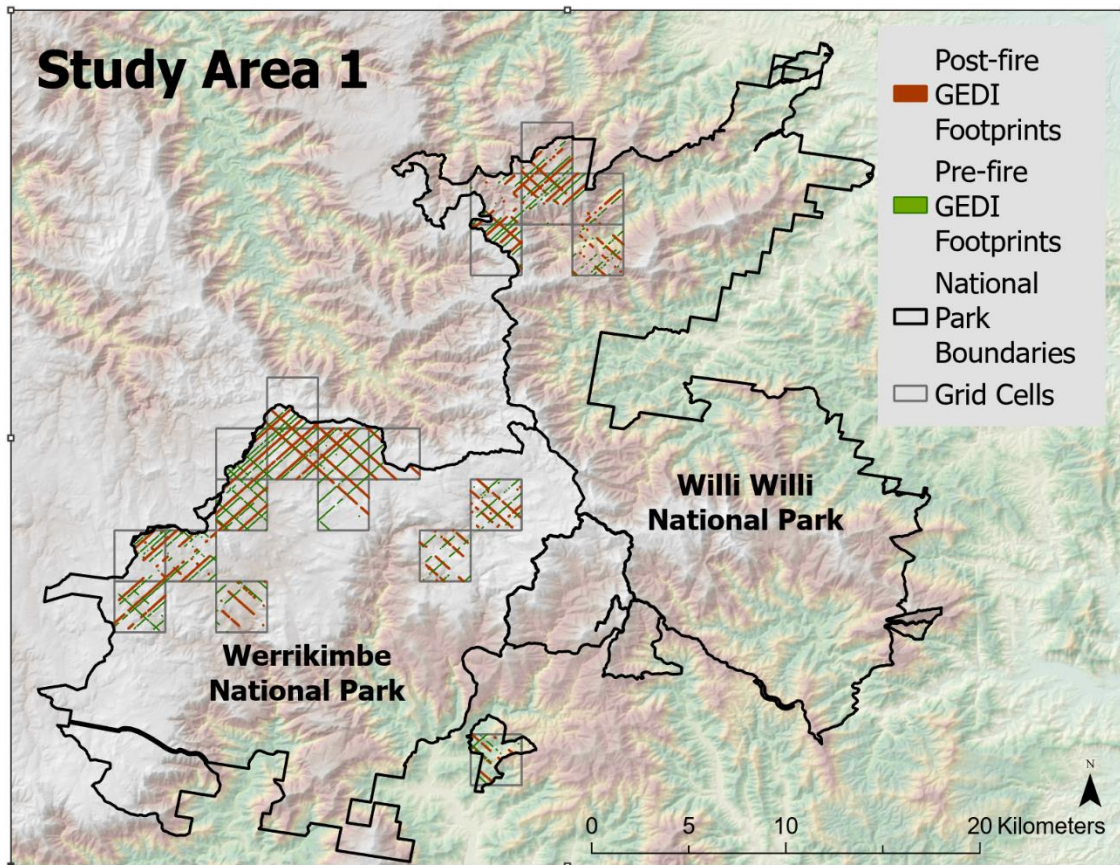


Figure 2 Study Area 1 (SA1) overview map with grid cells, pre-fire, and post-fire GEDI points over a digital elevation model with hillshade

Barrington Tops National Park is used as a control study area, referred to as Study Area 2 (SA2), its use as a control in this study is due to its lack of significant burns during the 2019-2020 fire season, with only 11% being considered fire-affected (Commonwealth of Australia, Department of Agriculture Water, and the Environment, 2020). Both SA1 and SA2 are Gondwana Rainforests and are located roughly 100 km apart on the east coast of New South Wales, Australia between the cities of Sydney (to the south) and Brisbane (to the north).

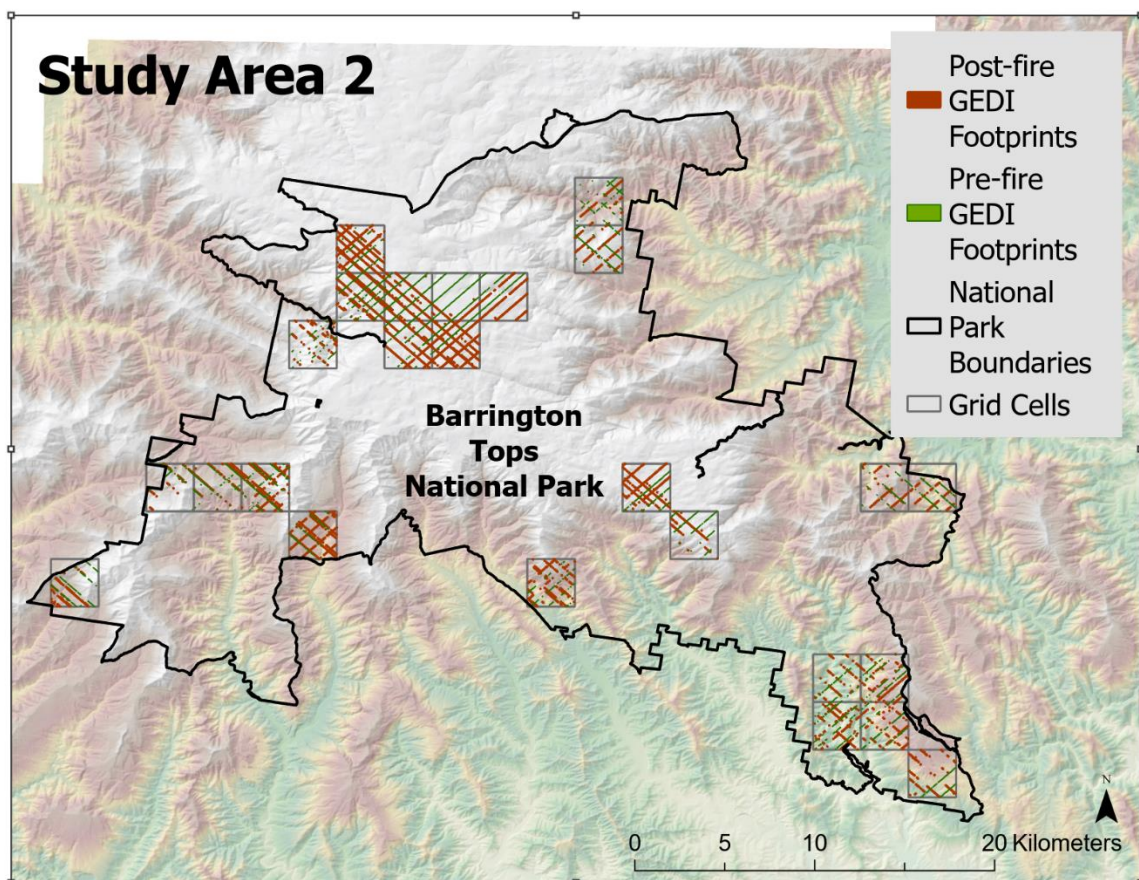


Figure 3 Study Area 2 (SA2) overview map with grid cells, pre-fire, and post-fire GEDI points over a digital elevation model with hillshade

4.2 MODIS Burned Area

Using Willi Willi National Park and Werrikimbe National Park as a conjoined primary study area, the MODIS Burned Area Product was used to determine exactly when and where burns occurred. Google Earth Engine (GEE) was used to access and download this data. The MODIS Burn Area Product is produced with daily surface

reflectance values at 500 meters spatial resolution from both Terra and Aqua platforms (Giglio et al., 2020). The algorithm uses surface reflectance values to identify areas of rapid change in conjunction with a vegetation index that is sensitive to burns, using bands 5 and 7. MODIS band 5 is located in the shortwave infrared (SWIR) region of the electromagnetic spectrum, from 1230-1250 nm. Band 7 also operates in the SWIR region, from 2105–2155 nm. See Table 1 for a complete list of the bands used in this study and related information. Atmospheric corrections have been applied to the associated band data. For areas the algorithm identifies as burned, the Julian day is assigned as the value for that pixel. Areas that are not flagged as burned have a value of 0. Inspection of the dataset across the study areas reveals when each study area experienced burning to determine the “before” and “after” dates for all other date-based data filtering.

Table 1 Satellite systems and the bands used in this study

Sensor	Band name	Wavelength (nm)	Spatial Resolution (m)
MODIS	5 – SWIR	1230-1250	500
	7 – SWIR	2105-2155	500
Landsat 8	4 – Red	630-680	30
	5 – NIR	845-885	30
	7 – SWIR	2100-2300	30

4.3 Landsat 8 spectral indices

GEE is used to access Landsat 8 data and generate the two spectral indices used in this study: the Normalized Burn Ratio (NBR) and the Normalized Difference Vegetation

Index (NDVI). The NBR is calculated using one NIR and one SWIR channel. For Landsat 8, the NIR reflectance is obtained with band 5, and the SWIR reflectance with band 7. The NBR results for Landsat 8 will have a spatial resolution of 30 meters. The NBR is then computed as follows (Hudak et al., 2007):

Equation 1 Normalized Burn Ratio (NBR) calculation

$$NBR = \frac{(NIR - SWIR)}{(NIR + SWIR)}$$

NDVI values will then be computed for each sensor for the pre-fire and post-fire data. NDVI requires a red reflectance band and a NIR reflectance band. Landsat 8 utilizes band 4 for recording red reflectance. The following equation is used for NDVI (Huang et al., 2021):

Equation 2 Normalized Difference Vegetation Index (NDVI) calculation

$$NDVI = \frac{(NIR - Red)}{(NIR + Red)}$$

These calculations were all performed in GEE. The NBR and NDVI were calculated twice each, once for pre-fire and once for post-fire. The pre-fire calculations used the monthly average values for September 2019; the earliest recorded burn date in the study area was in October. The post-fire calculations used the monthly average values for January 2020, as the last burn date for SA1 was in December 2019.

4.4 GEDI Data

The University of Maryland has led the GEDI mission since it was selected as a NASA Earth Ventures Instrument (EVI). GEDI was launched with the hope of furthering

our ability to characterize and understand the effects of climate change on ecosystem structures and dynamics. The instrument allows us to better quantify and understand carbon and water cycling processes. GEDI is based on the International Space Station (ISS), in the Japanese Experiment Module. It began collecting full waveform large footprint LiDAR data in 2019. GEDI data coverage is limited to 51.6 degrees North and South due to the orbital constraints of the ISS. GEDI's instrument consists of three lasers that emit 242 light pulses per second in the Near Infrared (NIR), at a wavelength of 1064 nm. One of the lasers is a coverage laser and is split into two beams, the other two lasers are full power beams, together producing four beams. Through the use of Beam Dithering Units (BDUs) the angle of the outgoing beams are shifted by 1.5 mrad ($1/1000^{\text{th}}$ of a radian). In total, this produces eight ground tracks of data, four being full power tracks and four coverage tracks. The distance between one track to the next, generated from the same beam at the same angle is 60 meters, this is the along track distance. The distance between the ground tracks produced by different beams or angles is 600 meters, this is the across track distance, see Figure 2. For a more in depth look at the GEDI instrument, readers should examine (Dubayah et al., 2020).

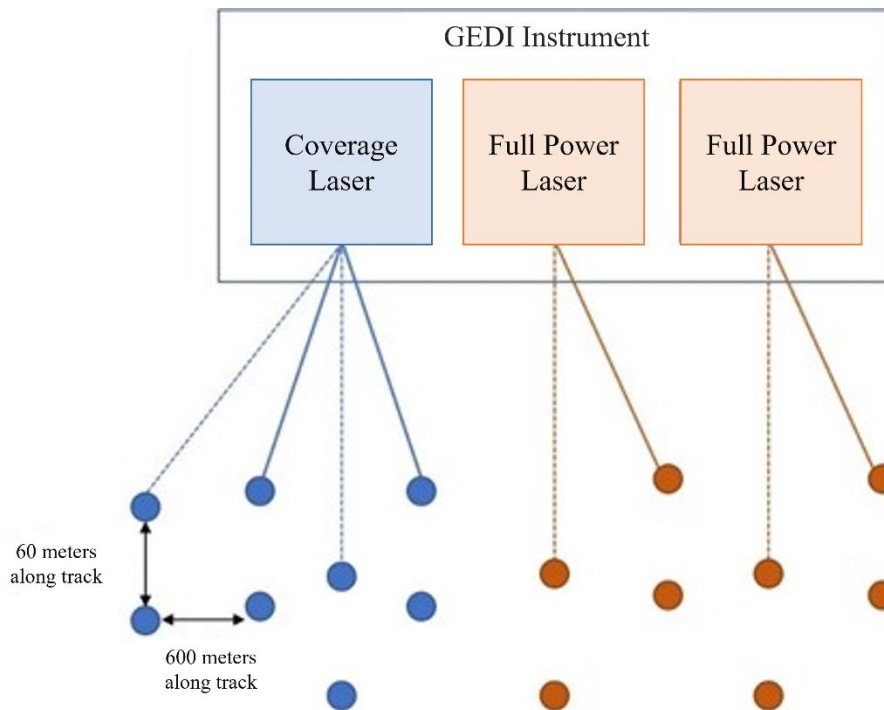


Figure 4 Illustration of the ground sampling pattern that GEDI uses. The dashed lines represent the result of dithering each beam to produce 8 different ground tracks of data. There is a 60 meter distance between GEDI footprints along track and a 600 meter distance between GEDI footprints across track.

Science data from the GEDI mission are all public and categorized at different levels. The algorithms, models, and physical theories behind these data products are elaborated on in the GEDI ATBD (Hofton & Blair, 2019). Level 1 (L1) and level 2 (L2) data are available through NASA's Land Processes Distributed Active Archive Center (LPDAAC). L1A being the raw waveforms and L1B being the geolocated waveforms. L2A provides ground elevation, top of canopy height, and relative height (RH) metrics. L2B offers canopy cover fraction (CCF) and CCF profile, plant area index (PAI), plant area volume density (PAVD), and foliage height diversity (FHD). All L1 and L2 data have a resolution of 25 m (GEDI footprint diameter). GEDI level 4 data (L4) can be

downloaded from NASA's Oak Ridge National Laboratory Distributed Active Archive Center (ORNLDAAC). L4A data provides users with aboveground biomass density (AGBD) estimates. Parametric models relating GEDI waveform relative heights metrics to field based AGBD estimates are used to derive the L4A data product (Dubayah, et al., 2021). This study uses L2A, L2B and L4A GEDI data, which was downloaded from the NASA EARTHDATA SEARCH tool. Using RStudio, the data was downloaded as hdf5 files (this was done using the httr, getpass and GEDI4R R libraries) and then converted into point shapefiles using python. Each point in the shapefile represents a GEDI footprint on the ground with a diameter of 25 meters. Each GEDI footprint point feature in the shapefile has information extracted from the L2A and L2B hdf5 files, including important statistics for evaluating vegetation structure. One of those being the relative height (RH) values at different returned energy quantiles.

An RH metric represents the height above the ground mode at which a specified quantile of energy is returned (Dubayah et al., 2020). To illustrate an example: an RH50 value of 10 (meters) would be indicative of a waveform having 50% of its energy returned to the sensor at a height of 10 meters above the ground. RH metrics can be calculated at any percentage between 0 and 100. This study uses RH50, RH75, RH90, RH95, RH98, and RH100. The only data used from the L4A product are the AGBD estimates.

Canopy cover is used to describe the spatially aggregated geometric properties of vegetation (Tang & Armston, 2019). Canopy cover as derived from GEDI observations is the canopy fractional cover (CFC) over the area where the sensor's laser is incident and is

the percent of the ground that is covered by the vertical projection of canopy material (Tang & Armston, 2019). GEDI derived Plant Area Index (PAI) is similar to the more commonly used Leaf Area Index (LAI), where LAI is defined as half of the total leaf area per unit ground surface (Chen et al., 1997), and PAI is one half of the total plant area per unit ground surface. PAI is different from LAI in that it includes the branches, stems and trunks of plants in addition to leaves (Tang & Armston, 2019). The difference in PAI and LAI tends to be small, and LAI values can be derived from GEDI PAI values. Plant Area Volume Density (PAVD) are vertical structure profiles with a vertical resolution of 5 meters (Tang & Armston, 2019) that indicate the areal density of vegetation for a given elevation or range of elevations (Griebel et al., 2015). PAVD profiles are calculated as a derivative of PAI for a specified height bin. Using vertical profiles of PAVD offer a 3-dimensional view of crown dynamics (Griebel et al., 2015). The PAVD vertical profile height bins used here are shown in Table 2. PAVD has implications for canopy carbon storage (Tang et al., 2012). Detailed information about PAI and PAVD can be found elsewhere (Tang et al., 2012). FHD serves as a method to measure the complexity of canopy structure, it is also referred to as Shannon’s Diversity Index. Higher FHD values can be associated with more complex forest structure (Tang & Armston, 2019). FHD can be used as an indicator for the quality of wildlife habitats.

Table 2 GEDI PAVD vertical profile height bins

Bin 1	Bin 2	Bin 3	Bin 4	Bin 5	Bin 6	Bin 7	Bin 8
0-5 meters	5-10 meters	10-15 meters	15-20 meters	20-25 meters	25-30 meters	30-35 meters	35-40 meters

GEDI AGBD estimates, from the L4A data product, are not published for all GEDI footprints. Only the highest quality footprints based on a selection criterion that includes the collection timeframe being within one of GEDI's "Golden Weeks" and that the footprints spatially overlap collection of previous LVIS lidar data. Additionally, GEDI footprints are only used if they meet standards for GEDI uncertainty metrics and quality flags. AGBD estimates are field-based values from different combinations of plant functional types and world regions. Parametric models using field-plot estimates of AGBD and GEDI RH metrics are used to derive the footprint level AGBD estimates. All AGBD values are in units of Mg/Ha (megagrams per hectare) (Dubayah, et al., 2022).

Prior to any filtering or processing, the GEDI footprints represented as points were converted to polygons by buffering the points by 12.5 meters to produce a circular polygon with a diameter of 25 meters, the same as the diameter of GEDI footprints on the ground. Values from satellite imagery, or other raster products, were then extracted based on the average value within each GEDI footprint. For each pre-fire or post-fire GEDI footprint, pre-fire NBR and NDVI values were assigned by averaging their values over the entire footprint polygon.

4.4.1 Filtering GEDI data for best results. The initial burn date from the MODIS Burned Area data product is used to determine the date for allocating data into the "pre-fire" or "post-fire" categories. All GEDI data recorded on or after that date, including GEDI footprints collected over the study area during an active burn, are treated as post-fire records. All GEDI data from before that date are considered pre-fire records. Areas

within the study area that did not experience burns are identified based on the MODIS Burn Area Product. GEDI data points overlapping these non-burn areas are flagged and not used in the statistical analyses.

The accuracy of GEDI data is influenced by the slope of the terrain it is incident upon. A 2020 study using GEDI data in Spain, reported higher RMSE values with higher slopes (Quirós et al., 2021). Similarly, a 2021 study discussed the waveform broadening effect associated with terrain slope and the impact it has on AGBD estimates (Ni et al., 2021). In accordance with these findings, GEDI footprints with an average slope value over 25° were removed from the study. The slope was generated from a 2-meter DEM from Australia's Elevation Foundation Spatial Data.

Additionally, GEDI data collected more than 270 days, or roughly nine months, before and after the recorded burn date were not used in the study. For the control area, where burns did not occur, the median burn date from SA1 was used as the determining date for limiting GEDI footprints used in SA2. Footprints collected within 270 days before and 270 days after the median burn date from SA1 were included.

4.5 Grid Cells

Since GEDI footprints will rarely directly overlap previously collected footprints, it is impossible to perform a direct comparison between pre-fire and post-fire collections in the same way it can be done with passive remote sensing systems that provide spatially continuous data products. Dividing the study area into grid cells and averaging the pre-fire and post-fire values in each cell allows for percent change comparison. Tessellation squares of 5 km² were created over SA1 with the ArcGIS Pro tool Generate Tessellation.

Only grid cells with a minimum of 50 GEDI footprints collected pre-fire and 50 post-fire were maintained and used in the study. All other grid cells and their overlapping GEDI points were not considered. This resulted in 20 grid cells with 2,196 pre-fire and 1,931 post-fire GEDI footprints included in the analysis. The same process applied to SA2 resulted in 25 grid cells having 2,245 pre-fire and 3,856 post-fire footprints.

As discussed in 4.4, GEDI AGBD estimates are not available for all footprints, resulting in a smaller dataset being used for that component of this study. Accordingly, SA1 AGBD analyses are based on 1441 pre-fire footprints and 879 post-fire footprints. To maintain a minimum of 50 pre-fire and post-fire points for each grid cell, the number of cells used in SA1 was reduced to 10, compared to the 20 cells used for the analysis of all other variables. For SA2, this did not reduce the number of grid cells used and minimally impacted the number of footprints available for processing, with pre-fire footprints numbering and 3,816 post-fire footprints.

5. RESULTS

Overall, the comparisons of pre-fire and post-fire GEDI derived metrics indicate significant changes in vegetation structure due to the 2019-2020 fires. Similarly, and as expected, the two satellite imagery derived indices also indicate intense burns. However, most GEDI metrics do not correlate with the indices and illustrate a possible weakness in applications that evaluate fire impacts solely based on such spectral indices. For each grid cell, the average value for all the GEDI footprints contained in it was calculated for each of the GEDI metrics and the extracted spectral indices' values: NBR, NDVI, RH50,

RH75, RH90, RH95, RH98, RH100, PAI, FHD, CCF, PAVD (for eight different vertical profile height bins), and AGBD.

5.1 Satellite indices

In SA1, average NBR values decreased by 61.3%, and NDVI values decreased by 46% (Figure 5). SA2, showed a 0% change in both average NBR and NDVI values.

These satellite metrics are not representative of the entire area; rather, they are a representative average based on their pixel values within the GEDI footprints used in the study. Percent change in NBR and NDVI were highly correlated, with a Pearson's correlation coefficient of 0.91. Surprisingly, neither were correlated with percent change in any of the studied GEDI metrics, positively or negatively (Table 3).

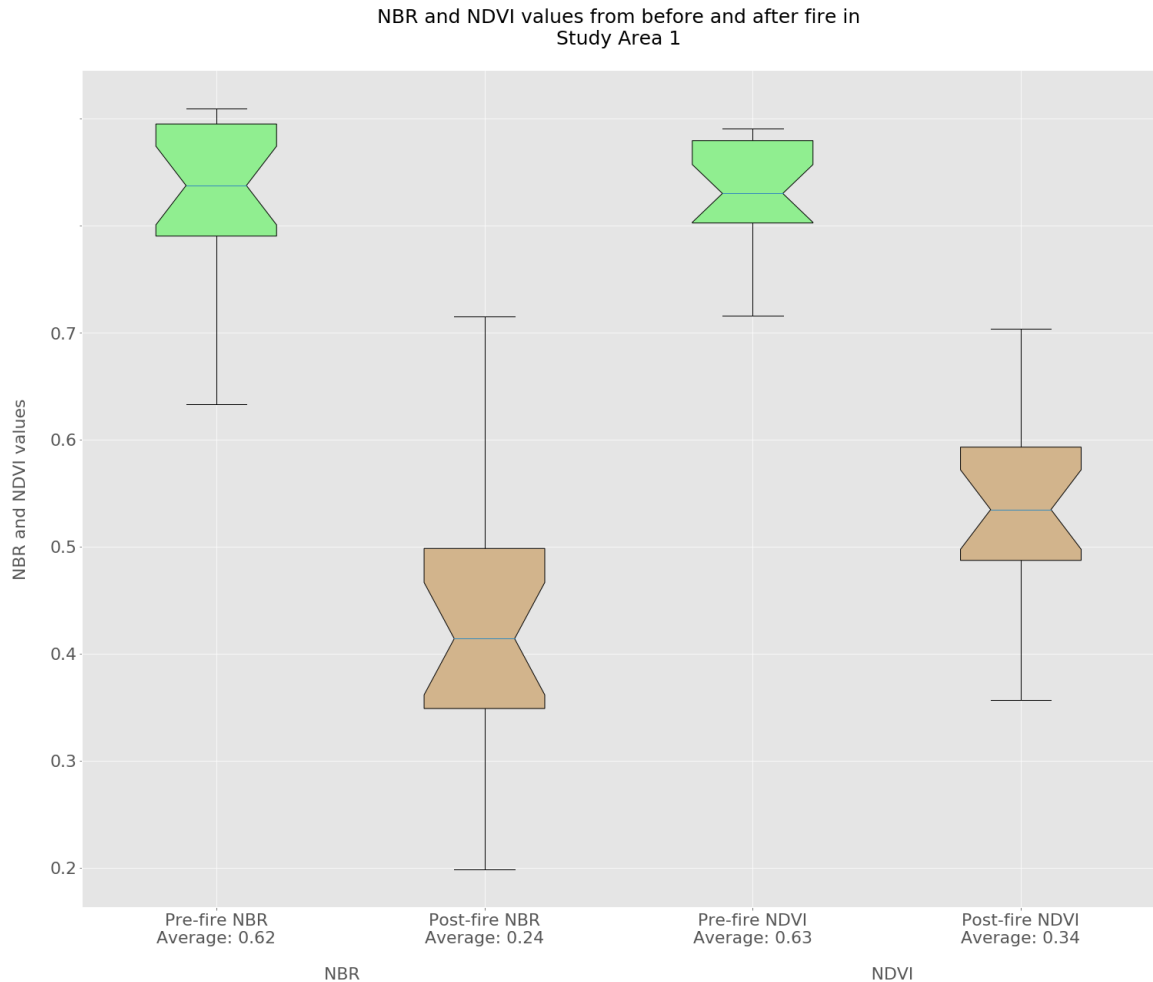


Figure 5 Boxplot of average Normalized Burn Ratio (NBR), on the left, and Normalized Difference Vegetation (NDVI), on the right, in SA1 with green representing pre-fire values and brown representing post-fire values

The pre-fire NDVI values are high and associated with dense vegetation. Post-fire NDVI values are in line with NDVI values for very sparse vegetation (Brown, n.d.). Pre-fire values are comparable to average NDVI values in the Amazon rainforest (Julien & Sobrino, 2009). Research has shown that differenced using NDVI (dNDVI) and NBR (dNBR) to evaluate burn severity score poorly in tall mixed forests, although no other indices performed higher (Tran et al., 2018).

5.2 GEDI vegetation metrics

Relative Height metrics:

Surprisingly, limited differences were observed between pre-fire and post-fire GEDI RH metrics. The largest changes were recorded in RH50 and RH75, which had average decreases of 12.7% and 5.1%. RH90, RH95, RH98, and RH100 all decreased by 1% or less (Figures 6 and 7). The control area, SA2, showed minimal changes in all RH metrics, with a range of -1.2 to -3.5% (Figures 8). Amongst different forest types, GEDI RH98 has been shown to have its lowest performance in tall tree forest stands and in high cover forest types (Wang et al., 2022); consequently, the observed changes in RH metrics and the related derived AGBD will incur some level of inherent errors.

Percent Change in GEDI RH metrics in Study Area 1

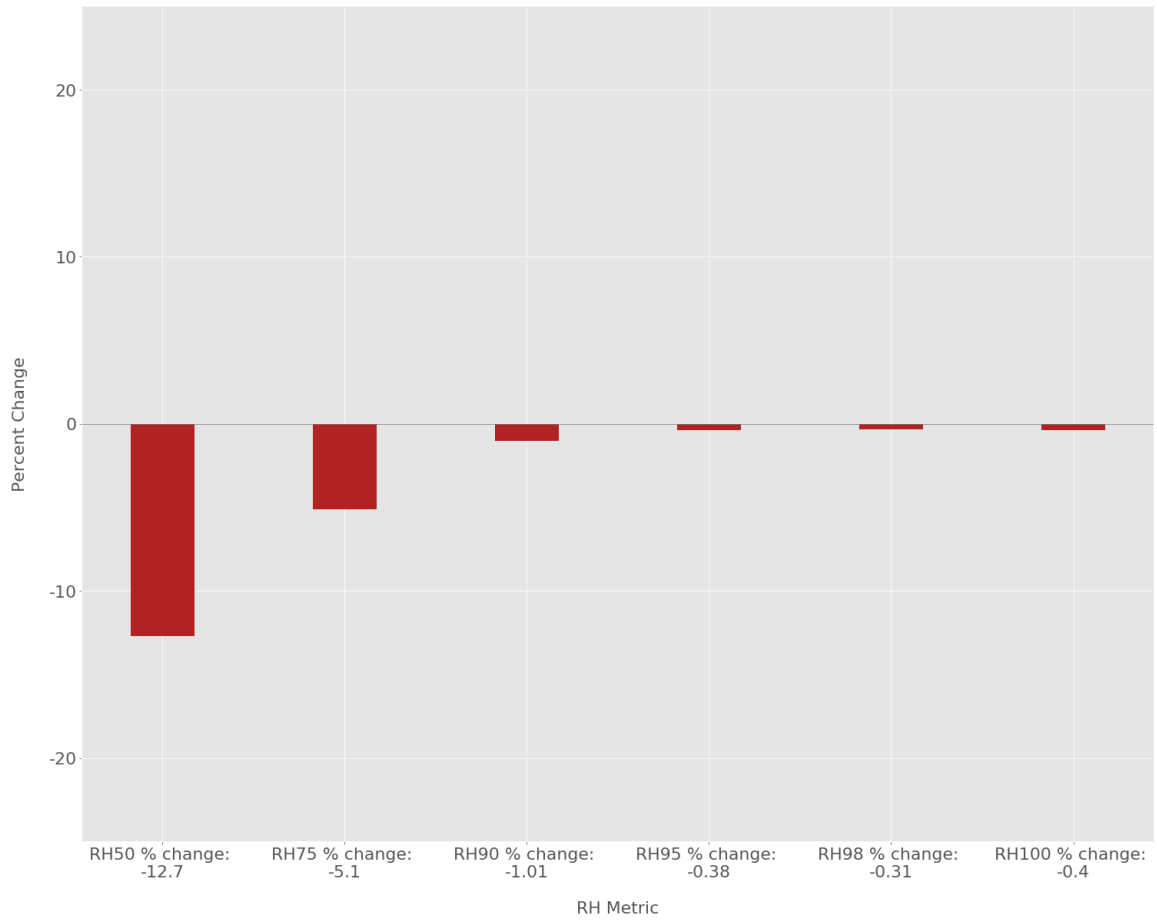


Figure 6 Percent change in each GEDI Relative Height (RH) metric in Study Area 1

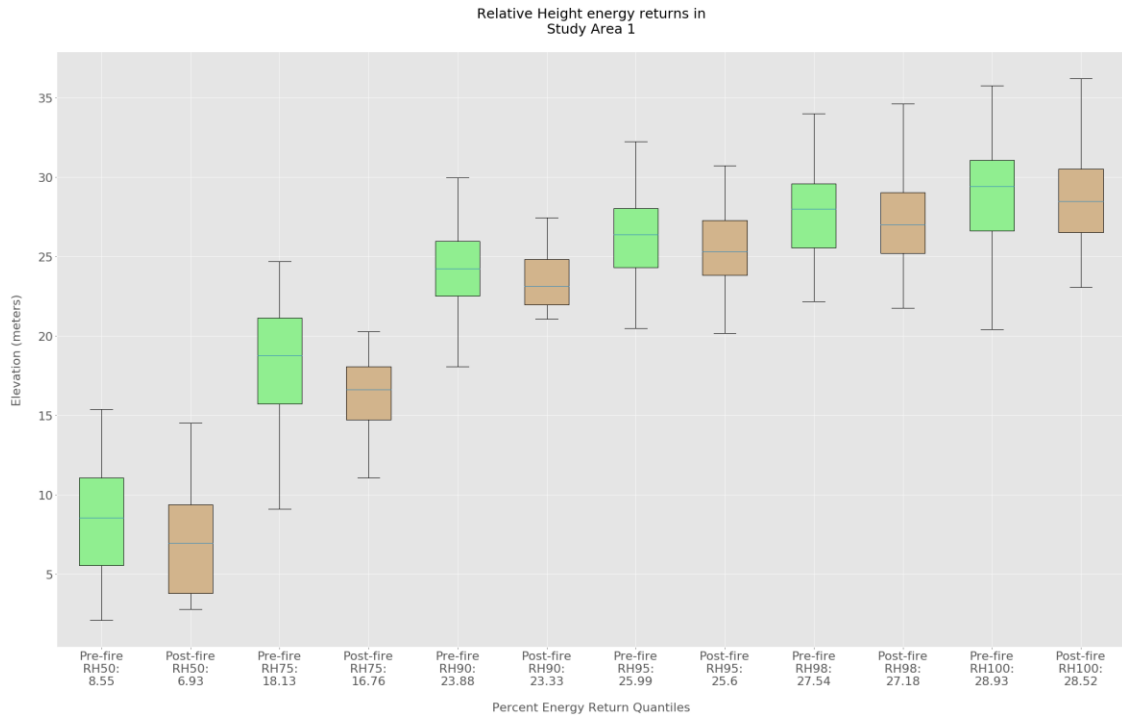


Figure 7 Boxplot of GEDI Relative Height (RH) metrics in Study Area 1

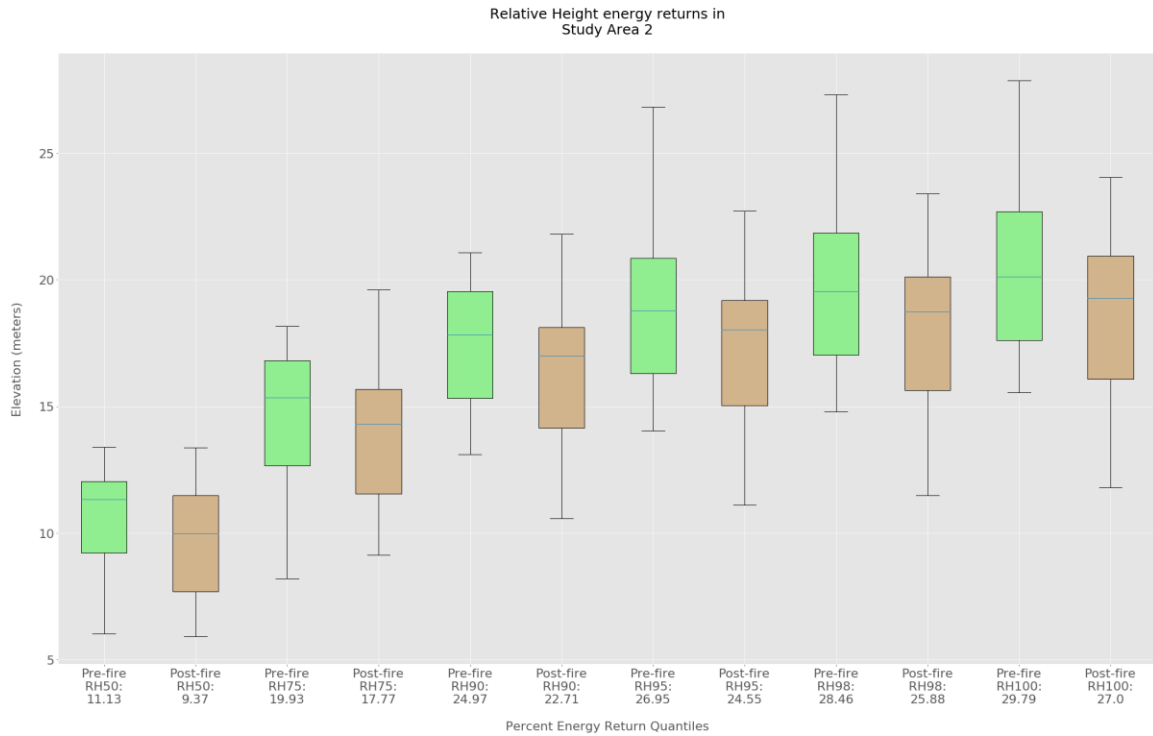


Figure 8 Boxplot of GEDI Relative Height (RH) metrics in the control area

Planet Area Index, Foliage Height Diversity and Canopy Cover Fraction:

In SA1, the average PAI value decreased by 19.8%, compared to the control, where PAI was observed to have increased by 1.68%. Average FHD decreased by 2.5% in SA1 and 0.51% in SA2. The Average CCF value in SA1 decreased by 15.15% while the control showed an increase of 0.58% (Figure 9). Supplemental figures regarding these metrics can be found in the appendix.

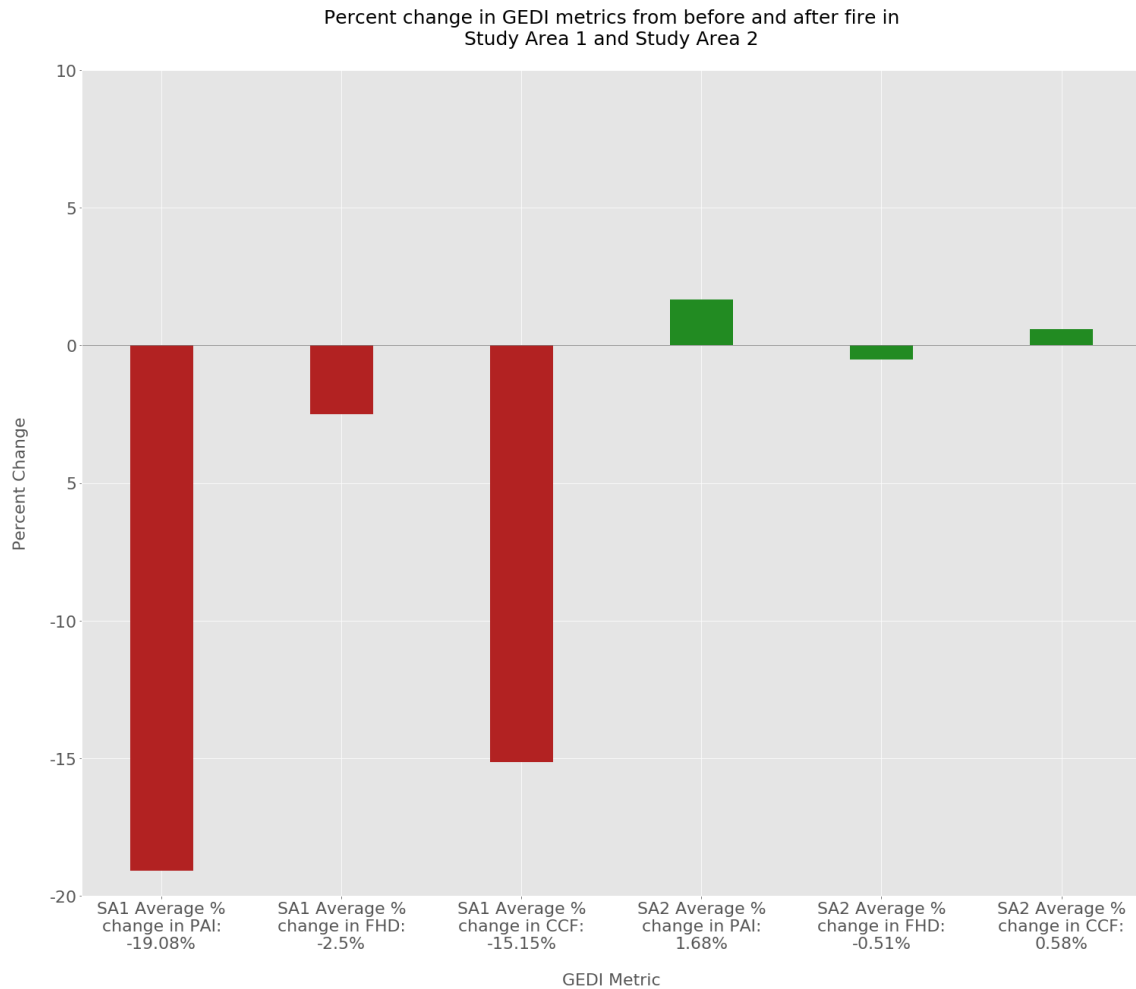


Figure 9 Comparison of the percent change in GEDI observed Plant Area Index (PAI), Foliage Height Diversity (FHD) and Canopy Cover Fraction (CCF) in SA1 (shown in red) and in SA2, the control area (shown in green)

Plant Area Volume Density:

GEDI vertical profiles of PAVD showed the most dramatic change in response to the fires. Vertical height profile bins 1-5 (0-25 meters) averaged a 20.9% reduction in PAVD (Figure 10), these same profiles also had the highest average values for PAVD (Figure 11). The average loss in each PAVD bin increases from bin 1 through bin 3 (0-15 meters), where the percent change peaks at -27.63. The percent change then steadily

decreases from bins 4 (15-20 meters) to bin 8 (35-40 meters). These trends are indicative of a fire that caused most of its damage in the understory and midstory of the forest, below the canopy. Conversely, the same analysis in SA2, the control, demonstrates changes in a forest spared from fire. The 15.7% increase in the 0-5 meter vertical profile bin (Figure 14 in appendix) could be attributed to new growth or differences in areas sampled by GEDI footprints. PAVD height bins above 40 meters were excluded from analysis as less than 50% of GEDI footprints in SA1 recorded any data for those values.

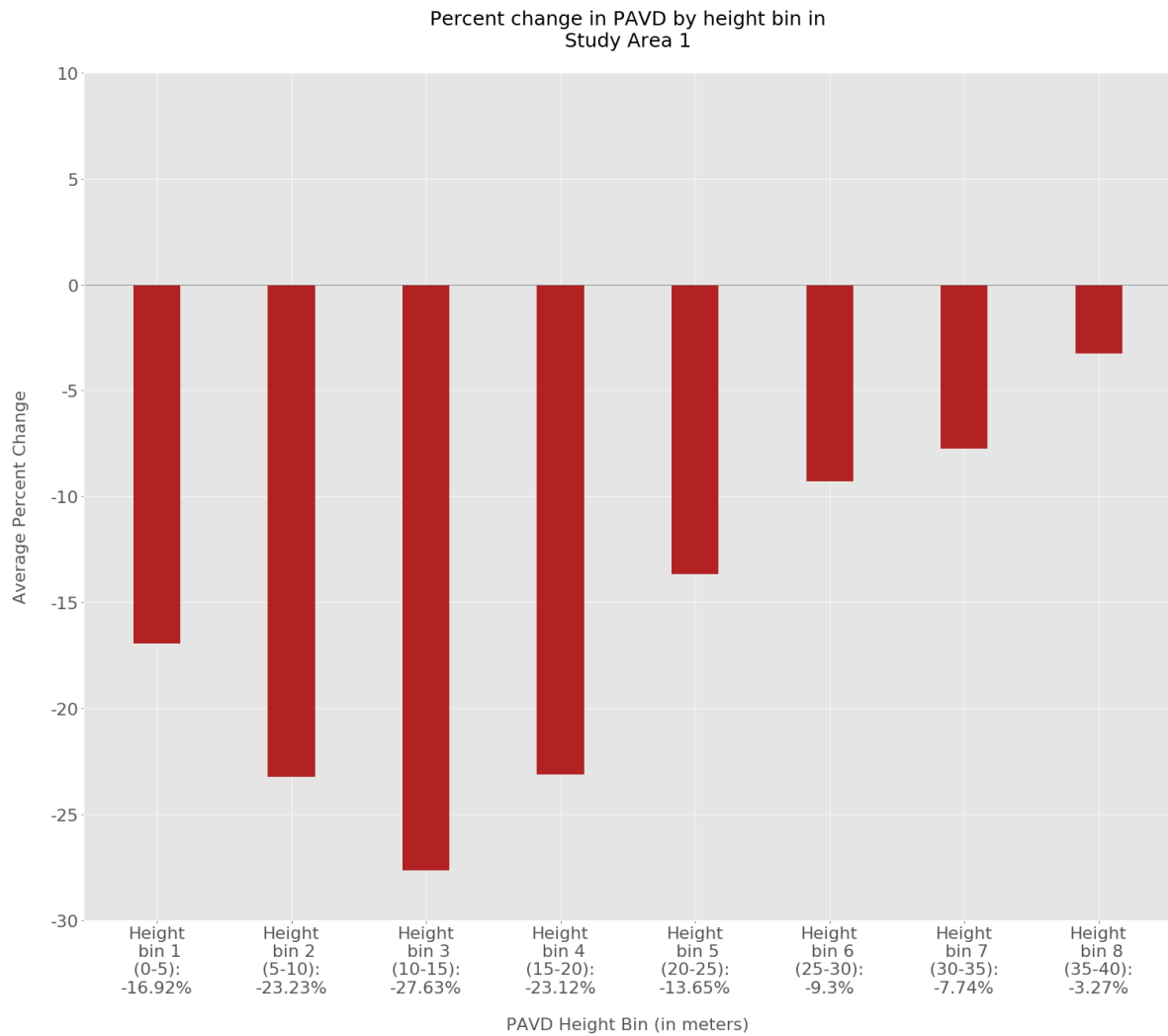


Figure 10 Percent change in GEDI Plant Area Volume Density (PAVD) by vertical profile height bin in Study Area 1 where each height bin has a vertical resolution of 5 meters and the bins range from 0-5 meters to 35-40 meters

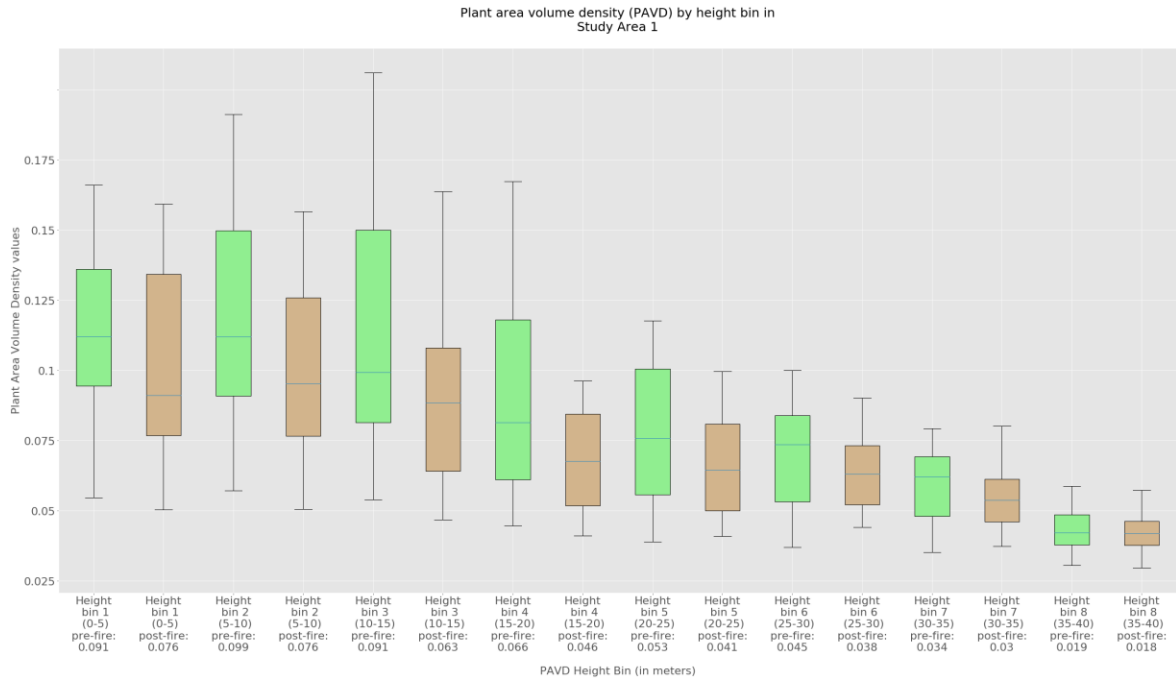


Figure 11 Boxplot of GEDI Plant area volume density (PAVD) showing pre-fire (green) and post-fire (brown) by vertical profile height bin in Study Area 1. Blue lines in boxes indicate the median value.

Above Ground Biomass Density (AGBD):

GEDI biomass (AGBD) estimates from L4A showed minimal changes. The average percent change in AGBD per grid cell was only -1.5% in SA1 (Table 3). While in SA2, the control area, percent change in AGBD was half that, at -0.76%. The GEDI footprints for which L4A AGBD data is available are more limited than the L2A data products used in this study. Since the algorithms used to generate the AGBD estimates are dependent on geographic variables and other GEDI data indicators, many of the L2A points used in analyzing other GEDI metrics did not have associated AGBD estimates (Duncanson et al., 2022; Kellner et al., 2022). GEDI AGBD estimations are mostly based on RH metrics, specifically RH98 (Duncanson et al., 2022), which also showed low percent change in SA1. The reliance on RH metrics and lack of inclusion of other GEDI

metrics, such as PAI and PAVD, could lead to limited observations of fire-induced changes in AGBD.

Table 3 Summary statistics from SA1 and SA2

***The Avg PC value represents the average percent change per grid cell, while the PC value represents the percent change between the pre-fire and post-fire averages for all grid cells**

<i>Metric</i>	<i>SA1</i>				<i>SA2</i>			
	Pre-fire	Post-fire	Avg PC*	PC*	Pre-fire	Post-fire	Avg PC*	PC*
<i>PAI</i>	2.31	1.80	-19.08	-22.08	2.64	2.53	1.68	-4.17
<i>FHD</i>	0.60	0.50	-2.50	-16.67	0.64	0.63	0.58	-1.56
<i>CCF</i>	3.08	2.99	-15.15	-2.92	3.05	3.01	-0.51	-1.31
<i>RH50</i>	8.55	6.93	-12.70	-18.95	11.13	9.37	-3.50	-15.81
<i>RH75</i>	18.13	16.76	-5.10	-7.56	19.33	17.77	-2.98	-10.84
<i>RH90</i>	23.88	23.33	-1.01	-2.30	24.97	22.71	-1.32	-9.05
<i>RH95</i>	25.99	25.60	-0.38	-1.50	26.95	24.55	-1.20	-8.91
<i>RH98</i>	27.54	27.18	-0.31	-1.31	28.46	25.88	-1.29	-9.07
<i>RH100</i>	28.93	28.52	-0.40	-1.42	29.79	27.00	-1.49	-9.37
<i>NBR</i>	0.62	0.24	-61.30	-61.29	0.08	0.08	0.00	0.00
<i>NDVI</i>	0.63	0.34	-46.00	-46.03	0.11	0.11	0.00	0.00
<i>PAVD 1</i>	0.09	0.08	-16.92	-16.48	0.99	0.11	15.70	-89.39
<i>PAVD 2</i>	0.10	0.08	-23.23	-23.23	0.11	0.11	8.77	0.93
<i>PAVD 3</i>	0.09	0.06	-27.63	-30.77	0.10	0.10	3.96	-3.06
<i>PAVD 4</i>	0.07	0.05	-23.12	-30.30	0.07	0.07	0.73	-2.78
<i>PAVD 5</i>	0.05	0.04	-13.65	-22.64	0.06	0.06	3.10	-5.08
<i>PAVD 6</i>	0.05	0.04	-9.30	-15.56	0.05	0.05	1.79	-6.00
<i>PAVD 7</i>	0.03	0.03	-7.74	-11.76	0.04	0.04	21.55	-12.50
<i>PAVD 8</i>	0.02	0.02	-3.27	-5.26	0.03	0.02	545.16	-18.52
<i>AGBD</i>	348.42	338.56	-1.50	-2.83	370.20	344.47	-0.76	-6.95

Table 4 Person’s correlation coefficients between pairs of variables in Study Area 1

	PC PAI	PC FHD	PC CCF	PC RH50	PC RH75	PC RH90	PC RH95	PC RH98	PC RH100	PC NDVI	PC NBR	PC PAVD (0-5m)	PC PAVD (5-10m)	PC PAVD (10-15m)	PC PAVD (15-20m)	PC PAVD (20-25m)	PC PAVD (25-30m)	PC PAVD (30-35m)	PC PAVD (35-40m)	PC AGBD
PC PAI	1																			
PC FHD	0.14	1																		
PC CCF	0.95	0.19	1																	
PC RH50	0.72	0.12	0.68	1																
PC RH75	0.46	0.67	0.59	0.64	1															
PC RH90	-0.02	0.73	0.08	0.23	0.77	1														
PC RH95	-0.12	0.73	-0.08	0.11	0.63	0.97	1													
PC RH98	-0.12	0.74	-0.12	0.08	0.56	0.93	0.99	1												
PC RH100	-0.11	0.75	-0.13	0.06	0.51	0.89	0.97	0.99	1											
PC NDVI	-0.11	-0.02	-0.03	0.04	0.24	0.54	0.51	0.46	0.38	1										
PC NBR	-0.04	-0.32	0.05	0.2	0.18	0.3	0.22	0.14	0.06	0.91	1									
PC PAVD (0-5m)	0.34	-0.52	0.4	-0.15	-0.37	-0.69	-0.77	-0.8	-0.8	-0.23	-0.05	1								
PC PAVD (5-10m)	0.58	-0.49	0.55	0.07	-0.29	-0.64	-0.7	-0.69	-0.68	-0.23	-0.08	0.92	1							
PC PAVD (10-15m)	0.92	-0.11	0.83	0.54	0.2	-0.22	-0.29	-0.28	-0.26	-0.13	-0.04	0.52	0.79	1						
PC PAVD (15-20m)	0.88	0.45	0.88	0.8	0.8	0.34	0.22	0.2	0.19	-0.07	-0.04	-0.01	0.21	0.69	1					
PC PAVD (20-25m)	0.77	0.54	0.75	0.82	0.8	0.37	0.28	0.27	0.27	-0.2	-0.18	-0.2	0	0.53	0.96	1				
PC PAVD (25-30m)	0.73	0.54	0.67	0.86	0.73	0.35	0.28	0.29	0.3	-0.19	-0.19	-0.29	-0.07	0.48	0.88	0.96	1			
PC PAVD (30-35m)	0.7	0.45	0.7	0.87	0.74	0.44	0.34	0.32	0.3	0.16	0.15	-0.23	-0.04	0.47	0.79	0.81	0.89	1		
PC PAVD (35-40m)	0.58	0.14	0.73	0.48	0.5	0.29	0.13	0.06	0	0.47	0.49	0.31	0.32	0.46	0.5	0.35	0.35	0.66	1	
PC AGBD	0.63	0.74	0.66	0.63	0.87	0.7	0.62	0.6	0.6	0.06	-0.08	-0.32	-0.14	0.39	0.86	0.87	0.82	0.76	0.47	1

Percent change in PAI was highly correlated with the PAVD height bins 3 and 4 (10-15m and 15-20m) with Pearson’s correlation coefficients of 0.92, 0.88, respectively. CCF, which is related to PAI, had similarly high coefficients to PAVD height bins 3 and 4: 0.83 and 0.88, respectively.

The highest Pearson’s correlation coefficient for percent change in NDVI were 0.54, 0.51, and 0.47 for RH90, RH95, and PAVD at the 35-40m height bin (bin 8), respectively. Aside from PAVD height bin 8, percent change for all other PAVD height bins had less than |0.23| correlation coefficient with percent change NDVI. Notably, PAVD height bins 2, 3 and 4 (5-10m, 10-15m, 15-20m), which exhibited the greatest

change amongst all studied GEDI metrics, had Pearson's correlation coefficients of –0.23, -0.13, and –0.07, respectively. Additionally, the percent change in AGBD was minimally correlated with a coefficient of 0.06.

In SA1, observed percent change in NBR over GEDI footprints was most closely correlated to GEDI PAVD height bin 8 (35-40m) and RH90, with Pearson's correlation coefficients of 0.49 and 0.3, respectively. PAVD height bins 2, 3, and 4 had coefficients of –0.08, -0.04, and –0.04, respectively. AGBD percent change had a correlation coefficient of –0.08. Percent change in GEDI AGBD correlates most closely with RH75, with a Pearson's correlation coefficient of 0.87. This alone is not surprising since GEDI AGBD estimates are based more on RH metrics than any other GEDI metrics. However, it is surprising and noteworthy that AGBD values have such a wide range of correlation coefficients with the PAVD vertical profile height bins. Coefficients are as low as –0.32 (0-5 meter height bin) and –0.14 (5-10 meter height bin) and as high as 0.87 and 0.86 (15-20 meter and 20-25 meter height bins). The PAVD in the 10-15 meter height bin, which recorded the highest average percent change, had a correlation coefficient of only 0.39 with AGBD. The correlation coefficients indicate that changes in PAVD are not reflected well in changes in AGBD.

6. DISCUSSION AND CONCLUSION

Remote sensing has been widely used to locate active fires, map fire perimeters, and estimate burn severity (Wooster et al., 2021), however, the results from this study demonstrate the new capability of GEDI to quantify the structural impacts of wildfires. The Gondwana Rainforests, a UN Educational, Scientific and Cultural Organization

(UNESCO) World Heritage site, are an ancient ecosystem, which have remained relatively unchanged since Australia began to break apart from Antarctica, 40 million years ago. The Gondwana Rainforests burn incredibly rarely, in fact most of the areas impacted by the 2019-2020 fires had never burned in recorded history (Fisher et al., 2021), and the long-term effects of the discussed fires are still unknown. No other place in the world has more threatened rainforest plant species than the Gondwana Rainforests of Australia (Kooyman et al., 2020). It has been determined that at least 113 endemic animal species had 30% or more of their range impacted by these fires (Commonwealth of Australia, Department of Agriculture, Water and the Environment, 2020). Lee et al. demonstrated the vulnerability of the Gondwana Rainforests to fires through the response of bird species to the 2019-2020 fires (Lee et al., 2022). They found that bird diversity was lower in burnt rainforests compared to unburnt rainforests. Laidlaw et al. found that satellite-based burn severity mapping in Gondwana Rainforests underestimated the severity of the fires' ecological impacts, largely because Rainforests are fire sensitive (Laidlaw et al., 2022), in opposition to the Eucalypt forests which are commonly subject to fires in Australia. They point out that detecting disturbances in tall, closed-canopy forests, like the Gondwana Rainforests are most reliable when there has been significant canopy loss. In an effort to quantify the species-level impacts of fires on wildlife in fire-sensitive environments, Law and coauthors found that the golden-tipped bat *Phoniscus papuensis* had lower occupancy rates in burnt rainforest, mostly due to loss of habitat (Law et al., 2022). New research has also shown that some rainforest plants are fire-resistant and influx on new species as shown through a 22% increase in woody plant

species richness during recovery following the fire. This was attributed to new seedlings and high resprouting rates (Baker et al., 2022). As climate change exacerbates the threat of new fires in these ecosystems, the importance of understanding the full extent of their impacts is important for the conservation of the Gondwana Rainforests.

GEDI, an active remote sensing system that acquired data both before and after the devastating 2019-2020 fires in Australia, offers a unique opportunity to use space-borne lidar data to investigate and quantify the impacts of forest fires on vegetation structure, biomass and thus potentially carbon emissions. This study shows that GEDI metrics are able to characterize the impacts of fires and illustrates that structural changes were more evident at lower levels of the canopy, rather than at top of canopy, which is the target most optical remote sensing techniques observe. Since GEDI is a sampling mission and the collection process produces spatially discontinuous footprints along tracks, there is an inherent amount of uncertainty introduced into the multi-temporal statistical analyses, as the time series of footprints do not overlap exactly. GEDI data must therefore be aggregated at various gridded levels to allow for spatial estimations and statistical comparisons (Patterson et al., 2019).

Research Question 1: How do GEDI observed changes in vegetation structure relate to spectral indices of burn severity?

In our study area (SA1), Landsat-derived NBR decreased at an average of 61.3%, and NDVI at 46% (Table 3), while the control showed no percent change in either satellite metric. While NDVI and NBR both showed changes in the spectral response of vegetation that are attributed to the damage caused by the fires, they do not correlate well

with any changes in GEDI structural metrics. The highest Pearson's correlation coefficient observed for percent change in NBR was 0.47, for percent change in PAVD vertical profile height bin 8 (35-40 meters). Percent change in NDVI had correlation coefficients of 0.54, 0.51, 0.46, and 0.49 for RH90, RH95, RH98 and PAVD bin 8, respectively (Table 4). The GEDI metrics with the highest correlation coefficients to the studied indices, while still low, are all tightly linked to vegetation structure at or near the top of canopy. The passive remote sensing techniques used to assess fire impacts, such as NBR and NDVI, only measure the changes in canopy reflectance from above. They effectively capture the loss of green, healthy vegetation and any accumulation of black soot from burnt vegetation. When observations are made over largely intact, green canopies, where the understory and or midstory are burnt, the observed spectral signature may not reflect structural changes below the canopy (Lentile et al., 2009).

Research Question 2: What differences can be observed in GEDI metrics between pre-fire and post-fire footprints? & Research Question 3: Which of the GEDI metrics offer the most insight into fire-induced changes in vegetation structure?

GEDI Relative Height (RH) metrics are commonly used for characterizing vegetation structure from large-footprint lidar and offer metrics related to biomass estimations. Each RH metric is defined as the distance between the detected ground elevation (the lowest mode in the full waveform for each GEDI footprint) and the n% accumulated waveform energy, where n is between 1 and 100 (Wang et al., 2022). RH50 exhibited the greatest percent change with an average of -12.70% followed by RH75 with percent change of -5.10%. RH90, RH95, RH98, and RH100 had average percent changes

between -1 and -0.3, as the magnitude of change decreases with each increase in accumulated energy. The overall magnitude of change in RH metrics is much lower than observed in other GEDI metrics. RH90 through RH100 represent vegetation close to or at the top of the canopy, while the most notable changes in PAVD occurred at lower levels of the forest. Therefore, minimal changes in high RH metrics are not surprising.

However, the lack of recorded change in RH metrics will impact AGBD estimations that rely exclusively on GEDI RH metrics during its calculation (discussed further below).

Plant Area Index (PAI) was observed to exhibit significant decreases, with an average percent change of -19.08 in SA1. PAI is intrinsically related to CCF and PAVD and their relationship is exhibited through the correlation analyses, where PAI has an average Pearson's correlation coefficient of 0.69 with highs of 0.92 and 0.88 at the 10-15 meter and 15-20 meter vertical profile bins, respectively, and a coefficient of 0.95 with CCF (Table 4). Derivations of these metrics are related to estimates of vertical canopy directional gap probability (Tang & Armston, 2019), for GEDI data this was derived based on Ni-Meister et al., using gap probability as a complement of vertical canopy profile (2001). However, it is poorly correlated with vertical profiles close to the ground and at the canopy level. Foliage Height Diversity (FHD) showed a minimal decrease due to fire in SA1, with an average of -2.5%. Since FHD offers insight into the heterogeneity of the vertical foliage profile, differences in sampling will have large impacts on this variable (Tang & Armston, 2019). Decreases in FHD can show a loss of complex canopy structure which can have ecological impacts such as the loss of biodiversity. However, surprisingly, FHD showed minimal change due to the fire. GEDI CCF essentially

provides the percent of the ground over which there is some canopy material, that being stems, leaves and branches (Tang & Armston, 2019). CCF values showed significant change with average percent changes of -15.15.

In this study, GEDI best captured changes in forest structure with the vertical profiles of Plant Area Volume Density (PAVD), effectively quantifying the density of vegetation in a 3-dimensional voxel at specific height elevations above the ground. GEDI PAVD values across all 8 vertical profile height bins averaged a decrease of 15.61%, with the 5-20 meter PAVD elevation profiles having an average decrease of 24.66%. These profiles also demonstrated the highest average PAVD values, showing that the fires severely impacted the most densely vegetated areas of the forest.

Observations of lower average percent change in the higher PAVD vertical profiles align with the observations by Laidlaw et al. (2022) who asserted that tall, closed-canopy forests can experience disturbances at lower levels of the forest without impacting the upper canopy. GEDI recorded changes to PAVD offer insight into how the vegetation structure was changed in a way that cannot be measured with passive remote sensing techniques which largely sense the top of canopy reflectance and not the lower strata of the forest. The manner in which fire sensitive environments, such as the Gondwana Rainforests, are impacted by and respond to these large wildfires can be revolutionized by the addition of structural metrics from space-based lidar.

Research Question 4: What changes do GEDI L4A above ground biomass density estimations show, and can they be used to derive carbon emissions estimations?

The models used to derive L4A, footprint level AGBD are developed per plant functional type (PFT) and geographic region and rely heavily on inputs from GEDI RH metrics (Duncanson et al., 2022). Calculations for AGBD introduce additional uncertainty, much of which comes from the fundamental uncertainties associated with the spatial distribution of above ground biomass (Kellner et al., 2022). AGBD in the main study area, SA1, showed an average percent change of only -1.5, dropping from an average of 348.42 Mg/ha to 338.56 Mg/ha. Percent change in AGBD is correlated with Pearson's correlation coefficients of at least 0.6 for all RH metrics, with the highest being 0.87 and 0.7 for RH75 and RH90, respectively. Despite these high correlation coefficients, it had a correlation coefficient of just 0.39 with the 10-15 meter PAVD height bin, which had the greatest reduction in vegetation density and the highest average PAVD pre-fire.

While relatively high correlations can be observed between AGBD and some PAVD vertical profiles, the minimal absolute change in AGBD raises concerns that it might not be accurately modelling the forest biomass in tall, closed-canopy rainforest containing significant midstory and understory. While Duncanson et al. try to limit the number of variables they use in the GEDI AGBD algorithms, RH98 is included in all of them and contributed the most information to the models' predictions (Duncanson et al., 2022). In undisturbed forests, these variables might give consistent and reliable indications of AGBD. However, forests that have experienced fires or other disturbances that impact the vegetation at varying sub-canopy heights may not exhibit notable changes in RH98 and these impacts will not be reflected in RH-derived AGBD.

Reliance on RH metrics in AGBD estimation algorithms may decrease the ability to predict changes in AGBD accurately and reliably. Other impactful events, such as the clear cutting of forests, where entire stands of trees are removed, will produce more reliable changes in AGBD. Assessing the impacts that changes in land use (in this case changes due to fire) have on atmospheric concentrations of carbon dioxide requires estimations of AGBD (Dubayah et al., 2022). In their process of deriving optimal models, lower RH metrics were included as potential variables. Perhaps forcing a low RH metric, such as RH50, into the algorithms, in the same manner that RH98 is forced, could introduce a viable means of ensuring AGBD estimates are able to reflect changes that occur in different levels of forestry. We recommend further research into AGBD algorithms that, in addition to RH metrics, consider the inclusion of other GEDI vegetation structure metrics that would accurately capture changes in carbon stocks derived from AGBD and consequently carbon dioxide emissions to the atmosphere.

Conclusion

At time of writing, this study was the first to demonstrate GEDI's ability to characterize fire impacts on forest structure, anywhere in the world, but we anticipate that this approach will become commonplace. GEDI PAVD vertical profiles between 5 and 15 meters exhibit the greatest impact, while the more well-known lidar derived RH metrics showed very limited impacts. As a result, RH-derived GEDI footprint level AGBD estimates did not capture the significant changes to biomass that took place during these fires. Consequently, GEDI AGBD based calculations for carbon emissions and carbon stock losses due to the fires will not be accurate. In order to be able to rely on

these data products to derive meaningful conclusions on carbon loss, further research will need to investigate the inclusion of GEDI metrics that are indeed sensitive to the impact of sub-canopy wildfires. We anticipate that GEDI data, or other full waveform lidar data, will in future, be regularly incorporated into assessments of fire severity and impact. This will contribute to developing an understanding of how Gondwana Rainforests respond to fires and how to best mitigate the impacts on carbon stock and wildlife habitat.

APPENDIX

Appendix of supplemental figures not included in main body.

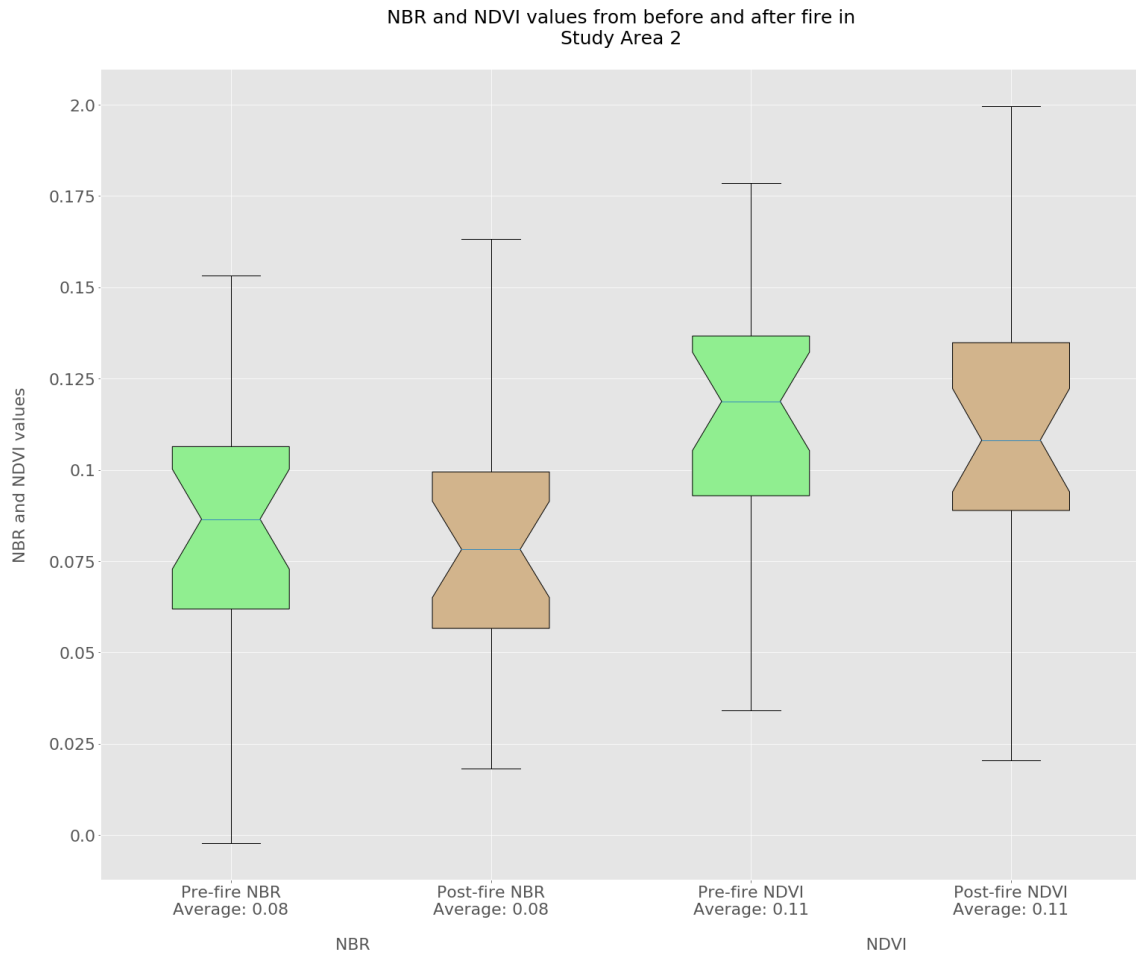


Figure 22 Boxplot of average Normalized Burn Ratio (NBR), on the left, and Normalized Difference Vegetation (NDVI), on the right, in SA2 with green representing pre-fire values and brown representing post-fire values

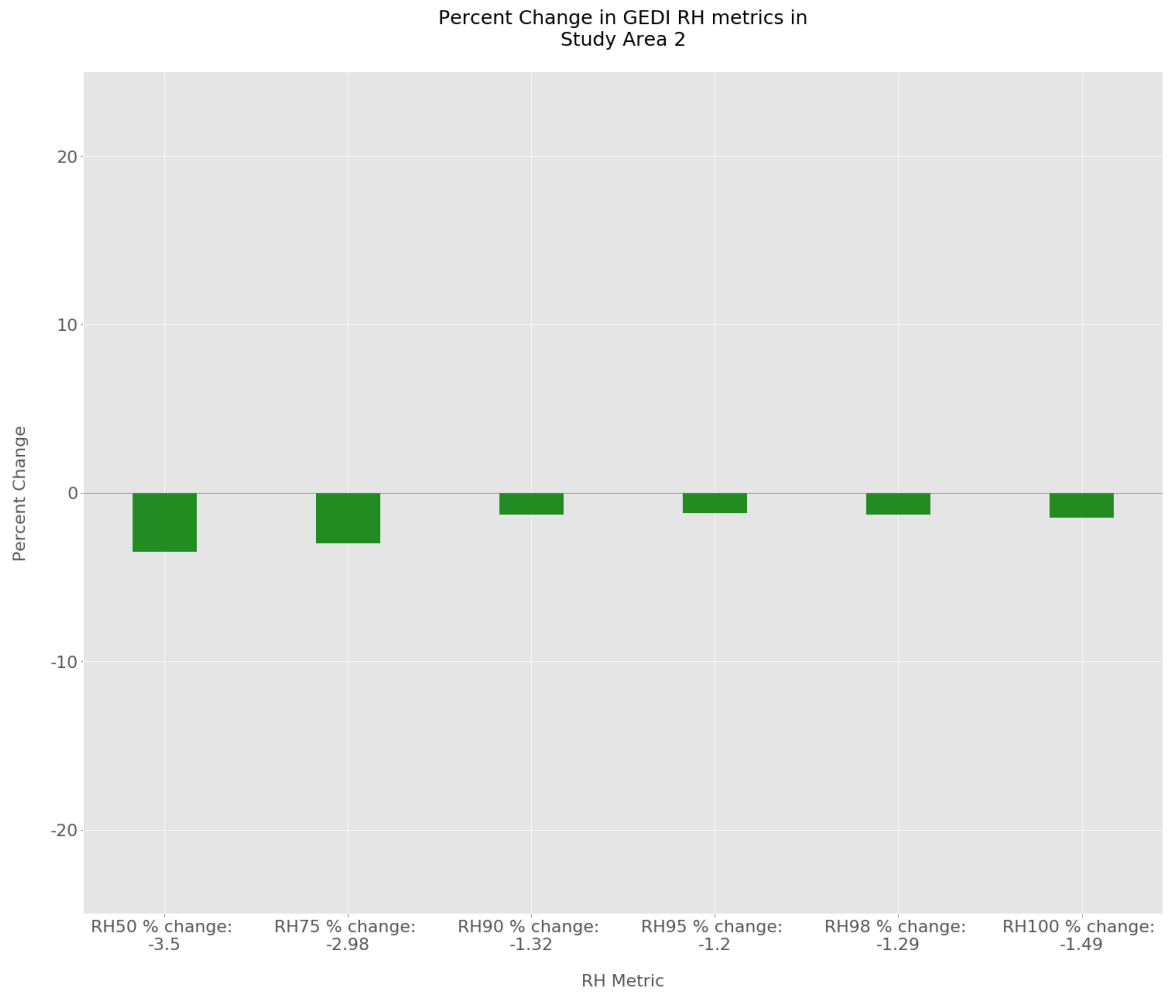


Figure 33 Percent change in each GEDI Relative Height (RH) metric in Study Area 2

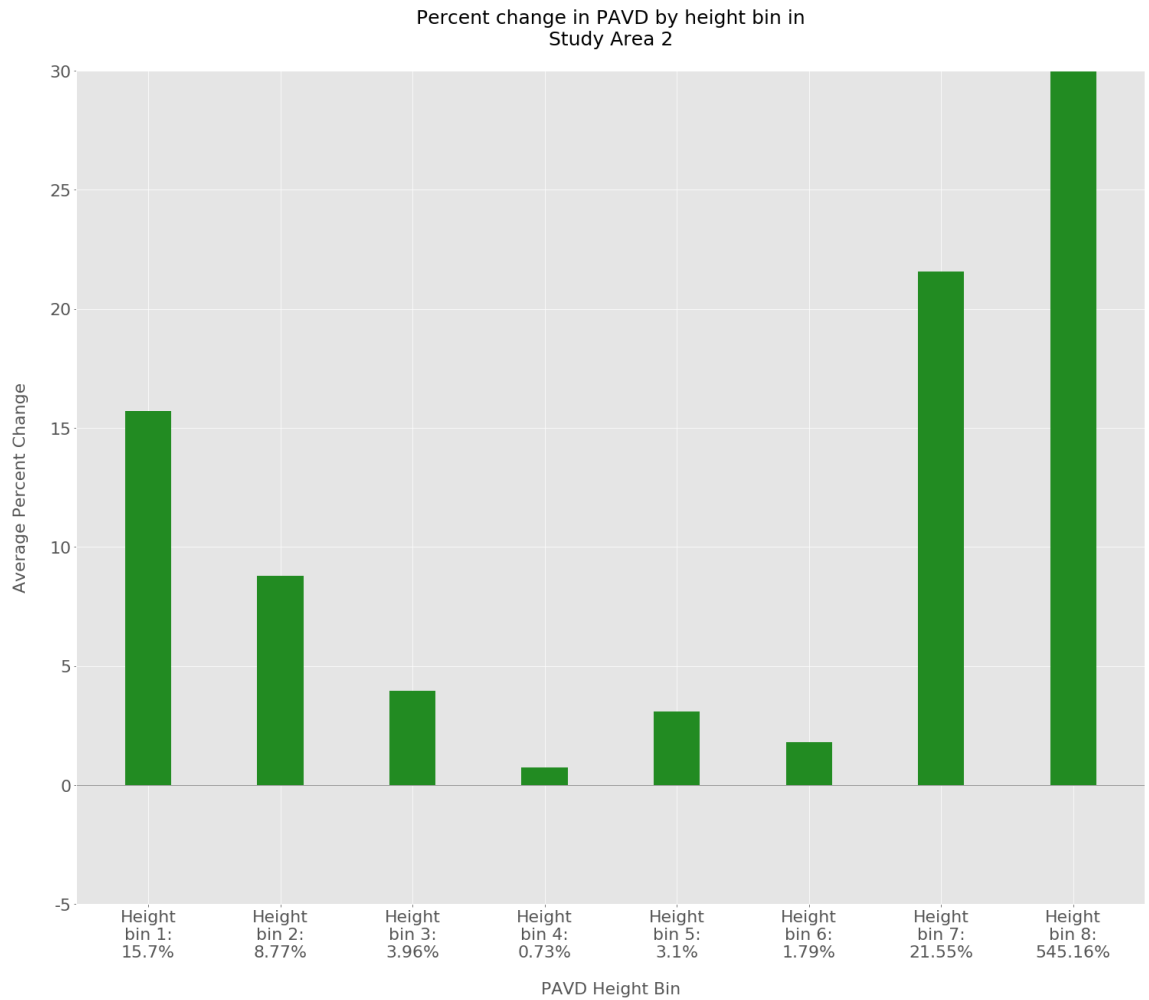


Figure 44 Percent change in GEDI Plant Area Volume Density (PAVD) by vertical profile height bin in Study Area 2 where each height bin has a vertical resolution of 5 meters and the bins range from 0-5 meters to 35-40 meters

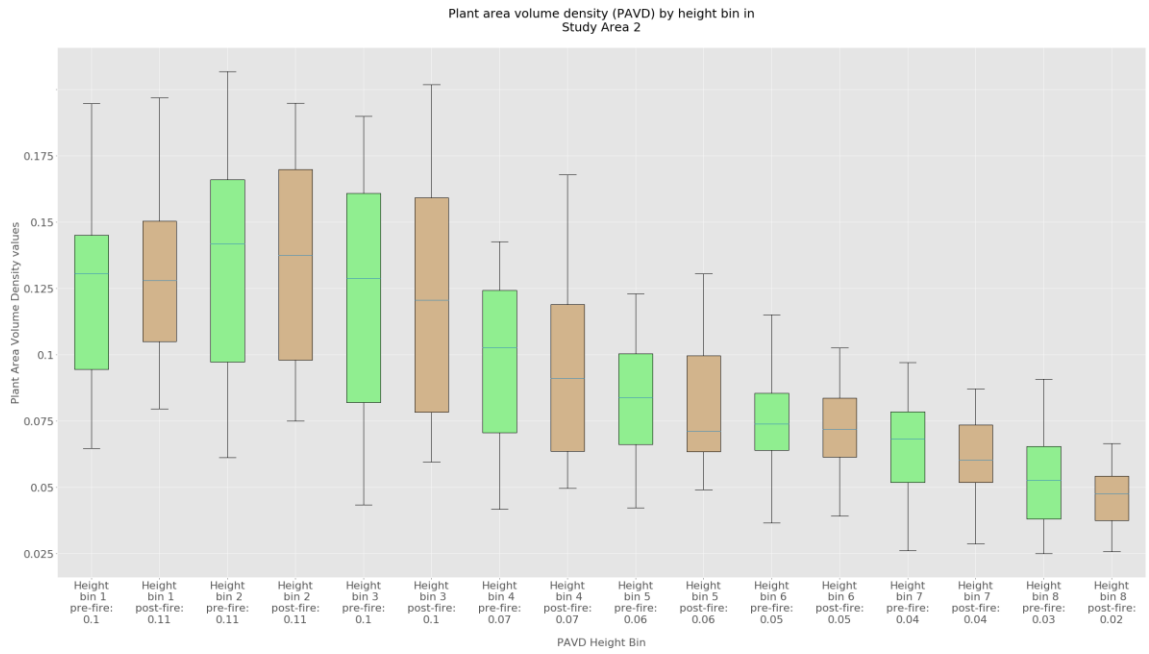


Figure 55 Boxplot of GEDI Plant area volume density (PAVD) showing pre-fire (green) and post-fire (brown) by vertical profile height bin in Study Area 1. Blue lines in boxes indicate the median value.

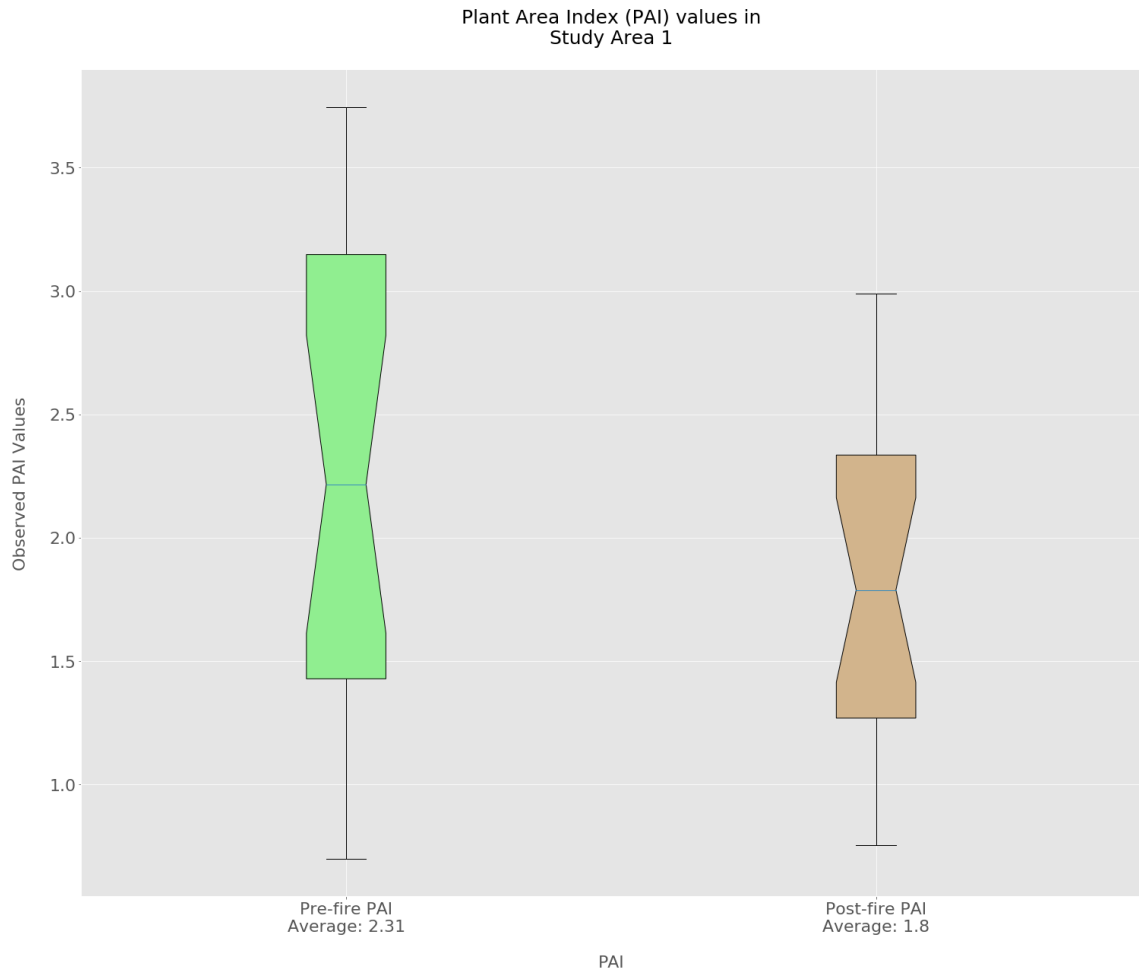


Figure 66 Plant Area Index (PAI) values from SA1

Foliage Height Diversity values from before and after fire in Study Area 1

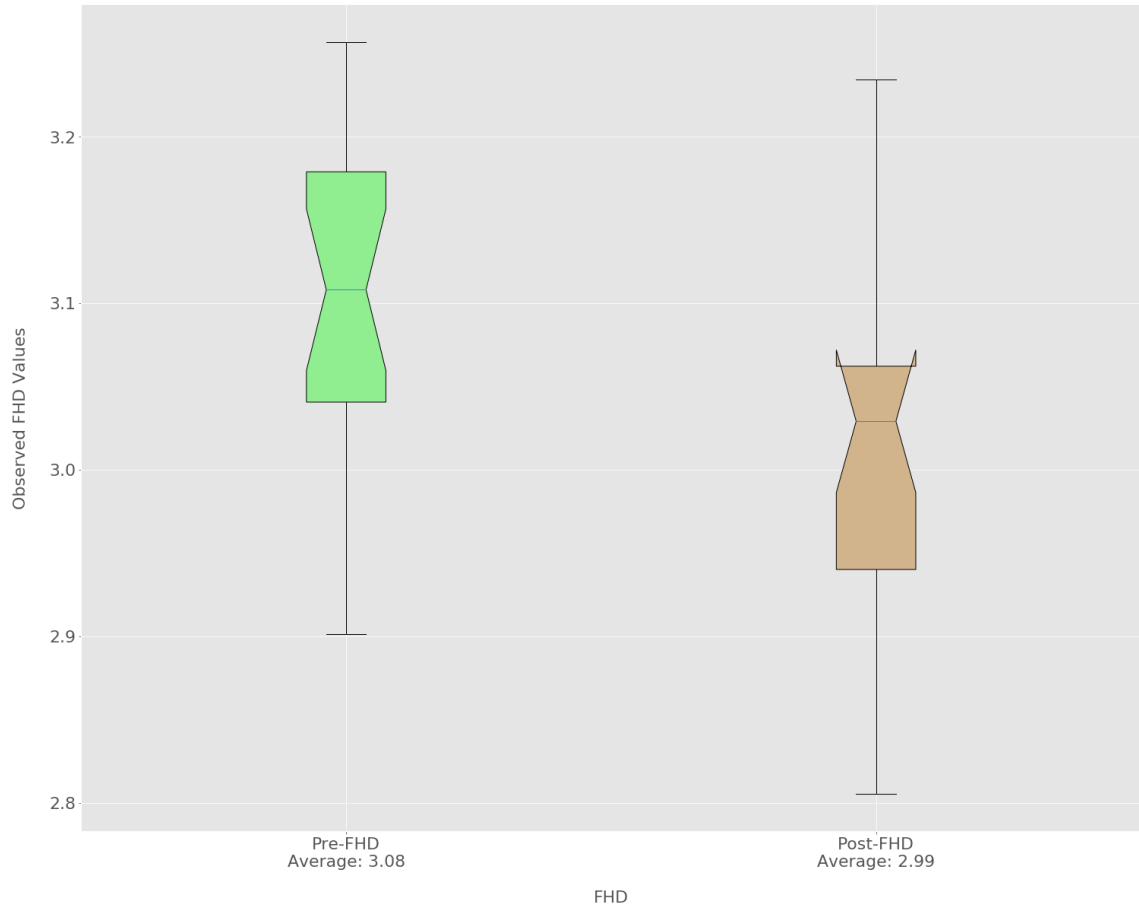


Figure 77 Foliage Height Diversity (FHD) values from SA1

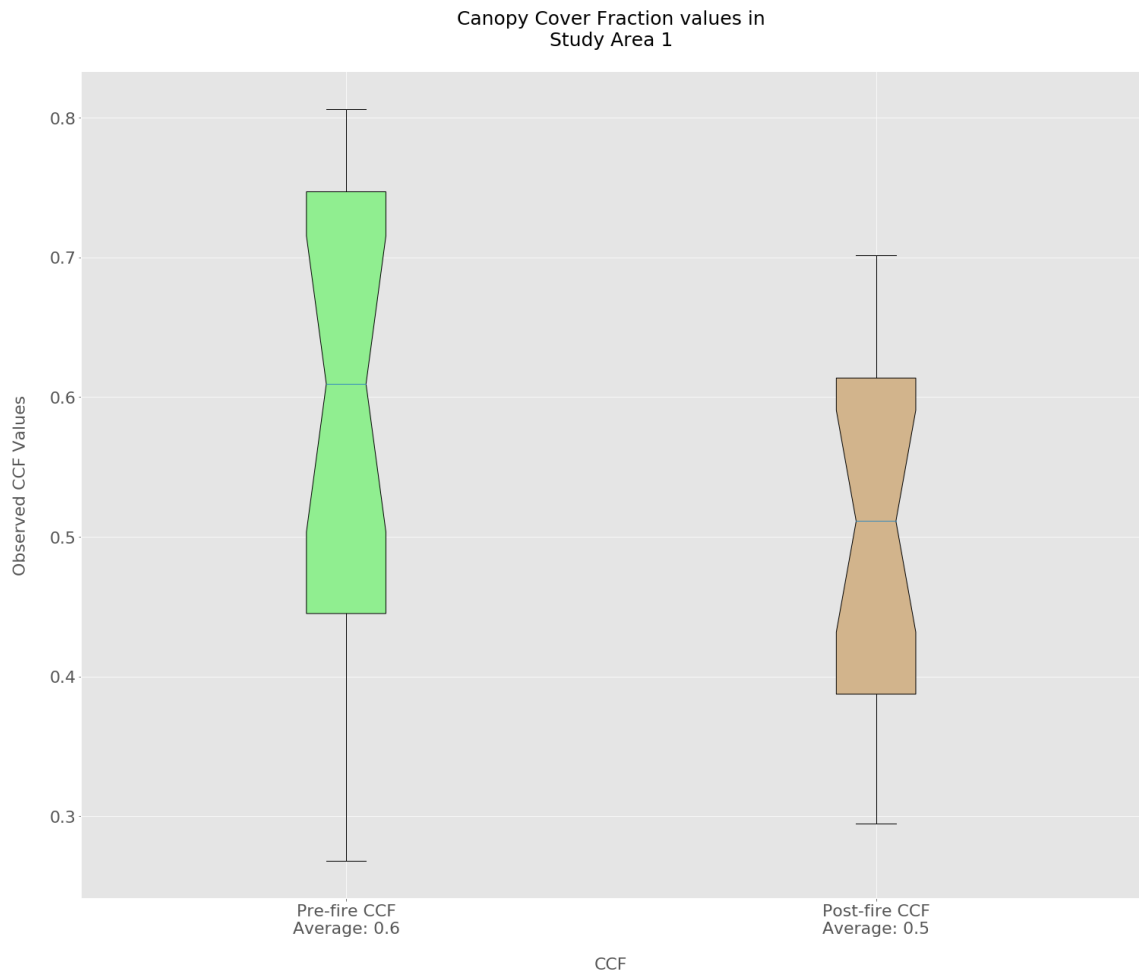


Figure 88 Canopy Cover Fraction (CCF) values from SA1

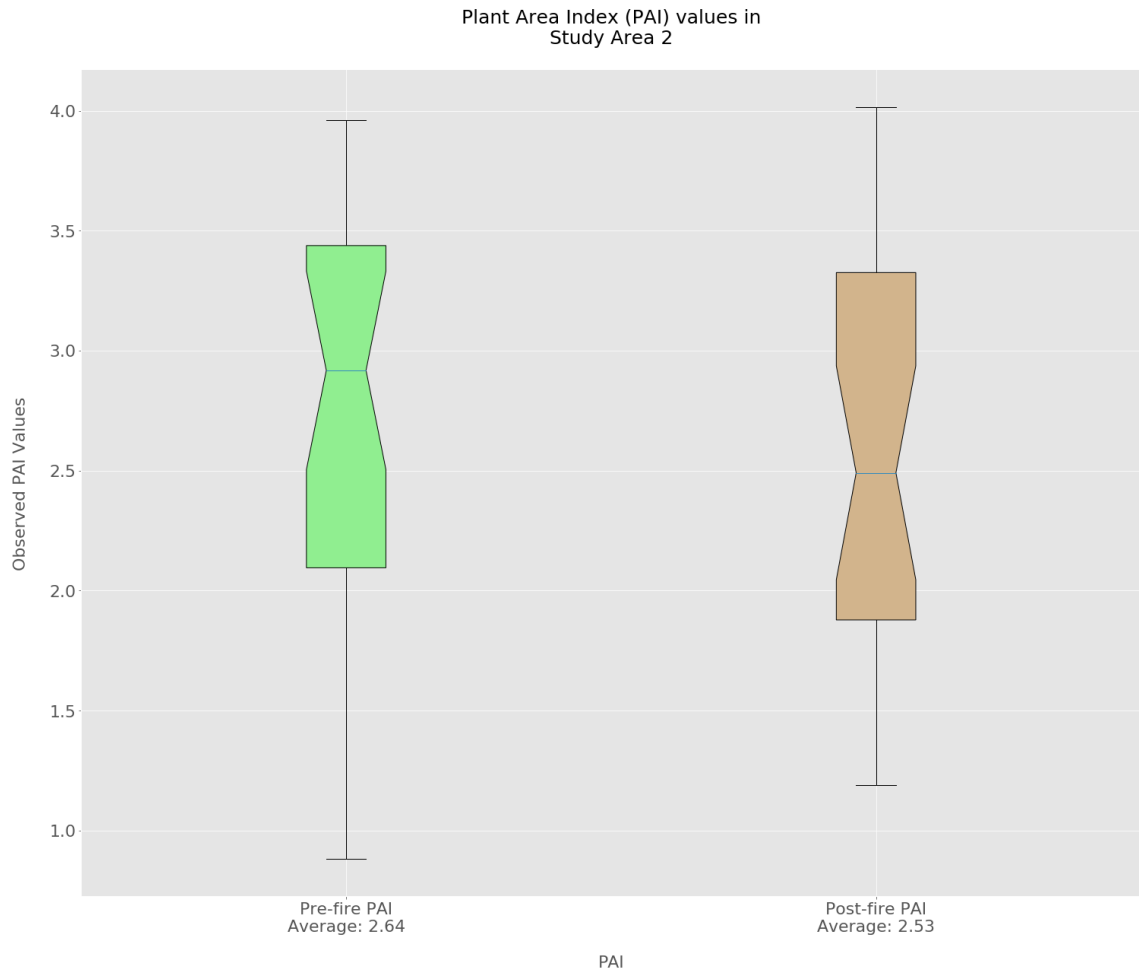


Figure 99 Plant Area Index (PAI) values from SA2

Foliage Height Diversity values in Study Area 2



Figure 20 Foliage Height Diversity (FHD) values from SA2

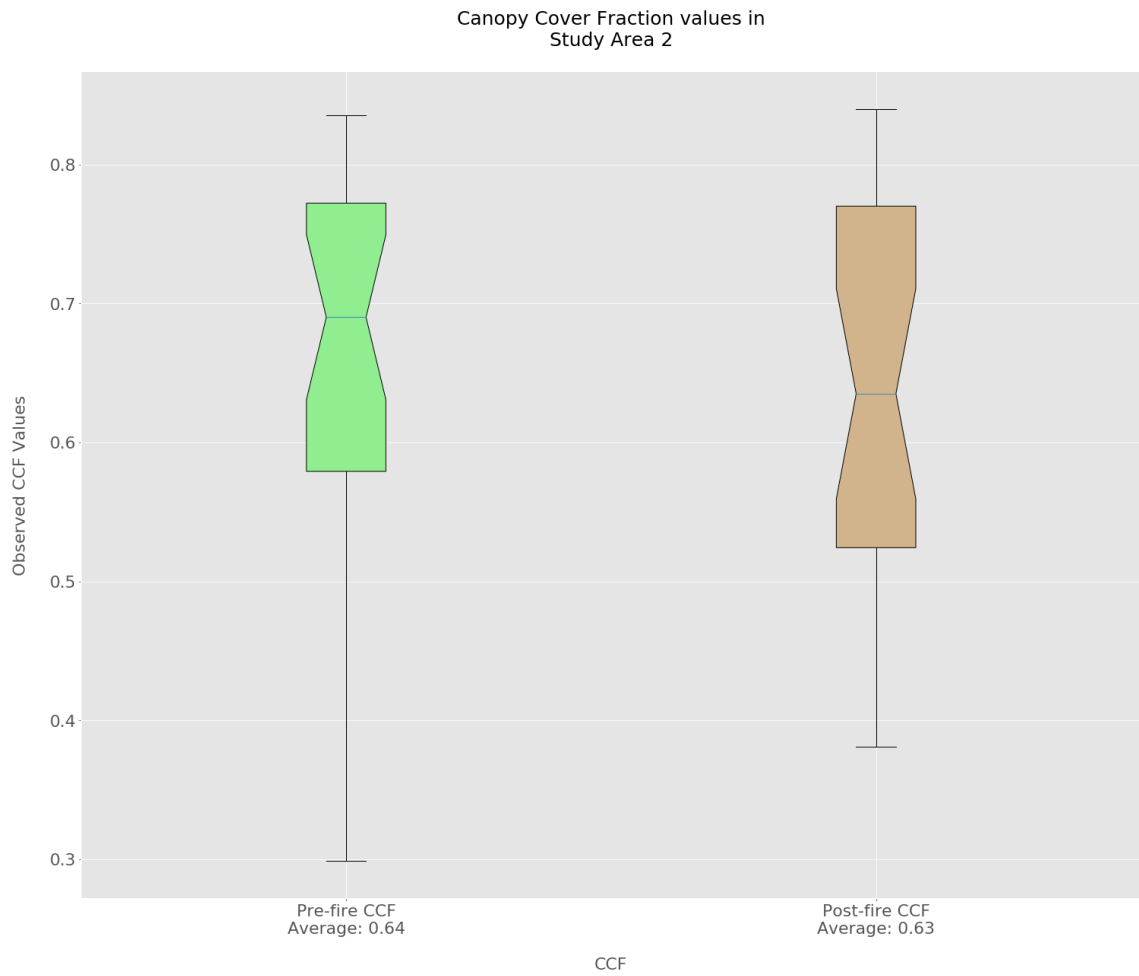


Figure 21 Canopy Cover Fraction (CCF) values from SA2

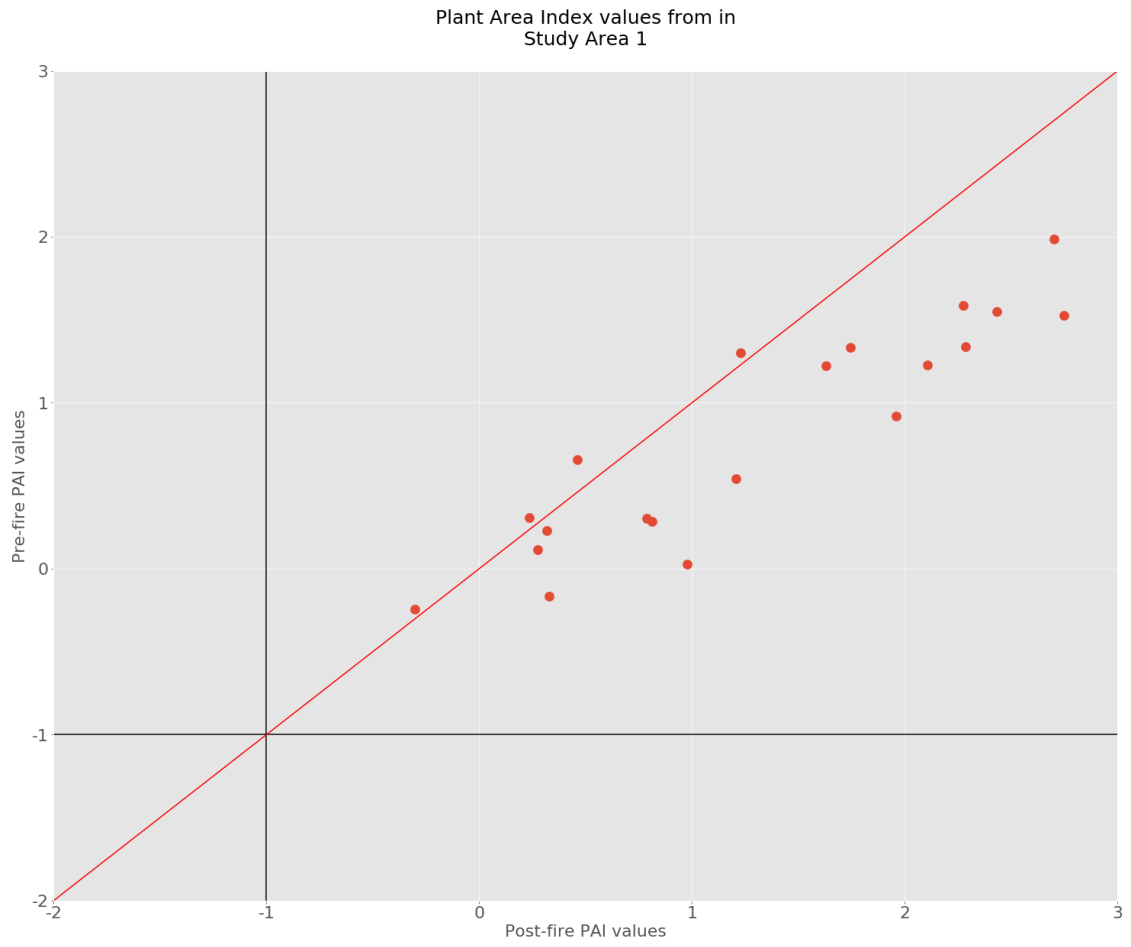


Figure 22 Plant Area Index (PAI) scatterplot, SA1

Foliage Height Diversity Values values in Study Area 1

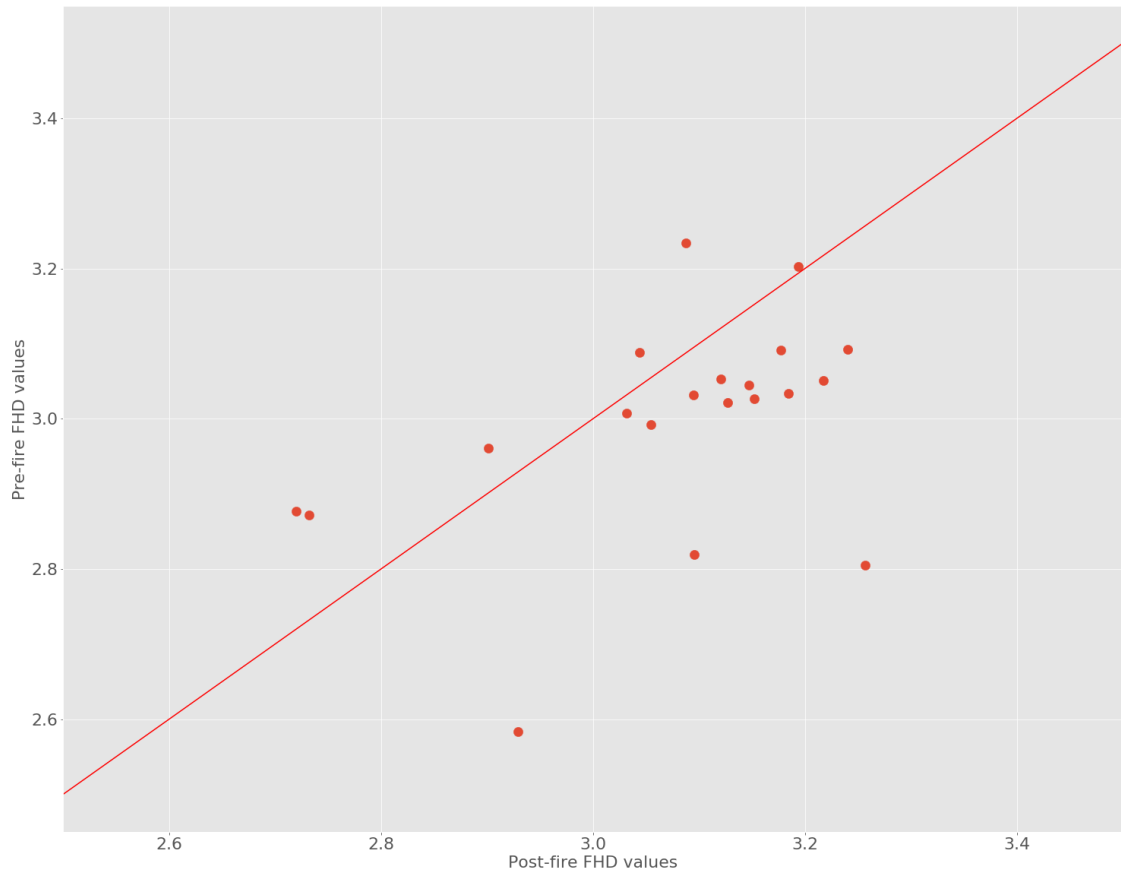


Figure 23 Foliage Height Diversity (FHD) scatterplot, SA1

Canopy Cover Fraction Values values in
Study Area 1

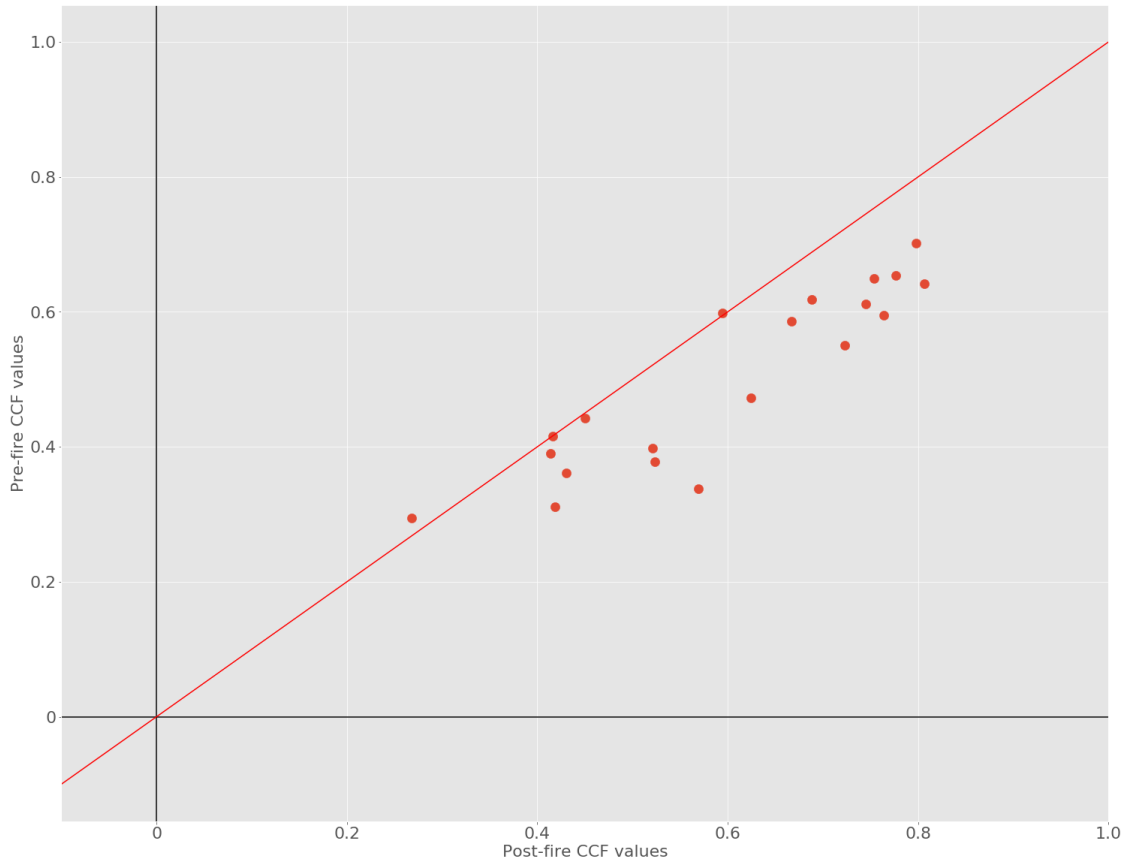


Figure 24 Canopy Cover Fraction (CCF) scatterplot, SA1

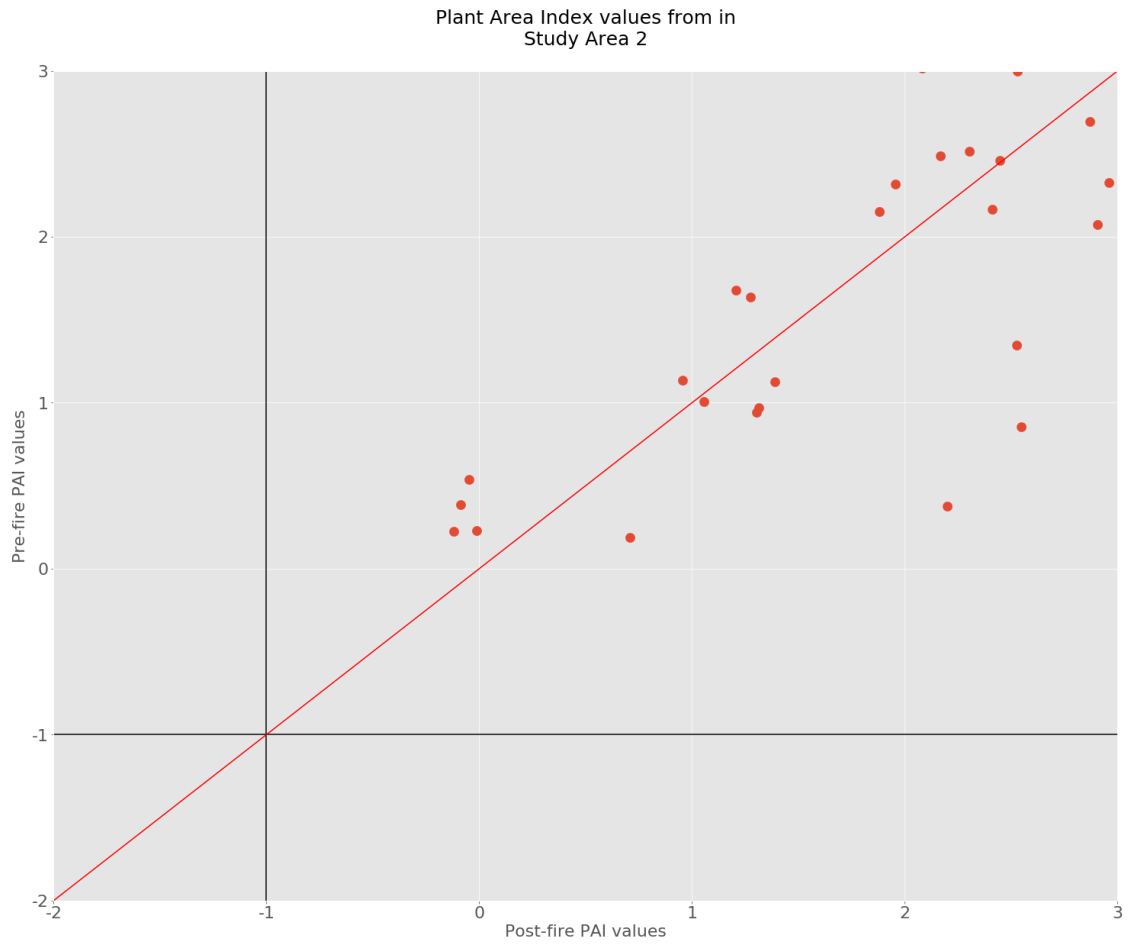


Figure 25 Plant Area Index (PAI) scatterplot, SA2

Foliage Height Diversity values in Study Area 2

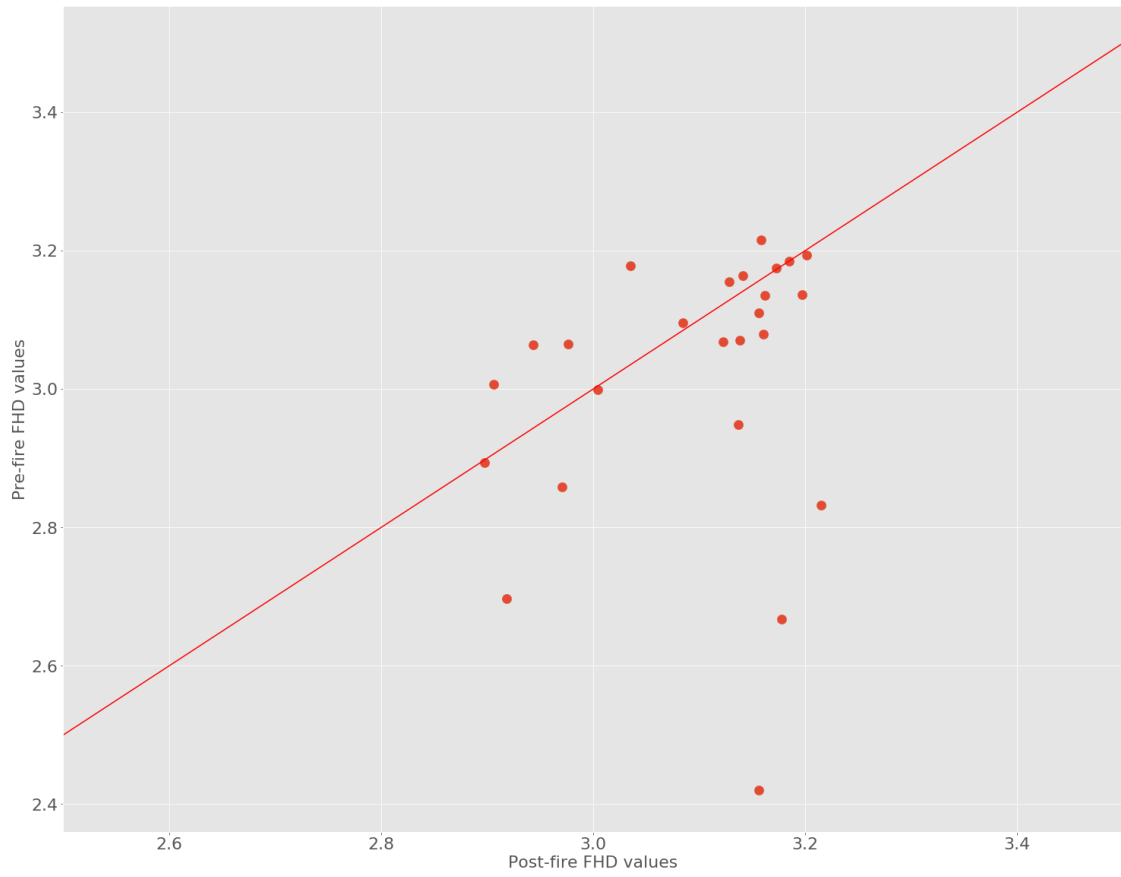


Figure 26 Foliage Height Diversity (FHD) scatterplot, SA2

Canopy Cover Fraction Values values in Study Area 2

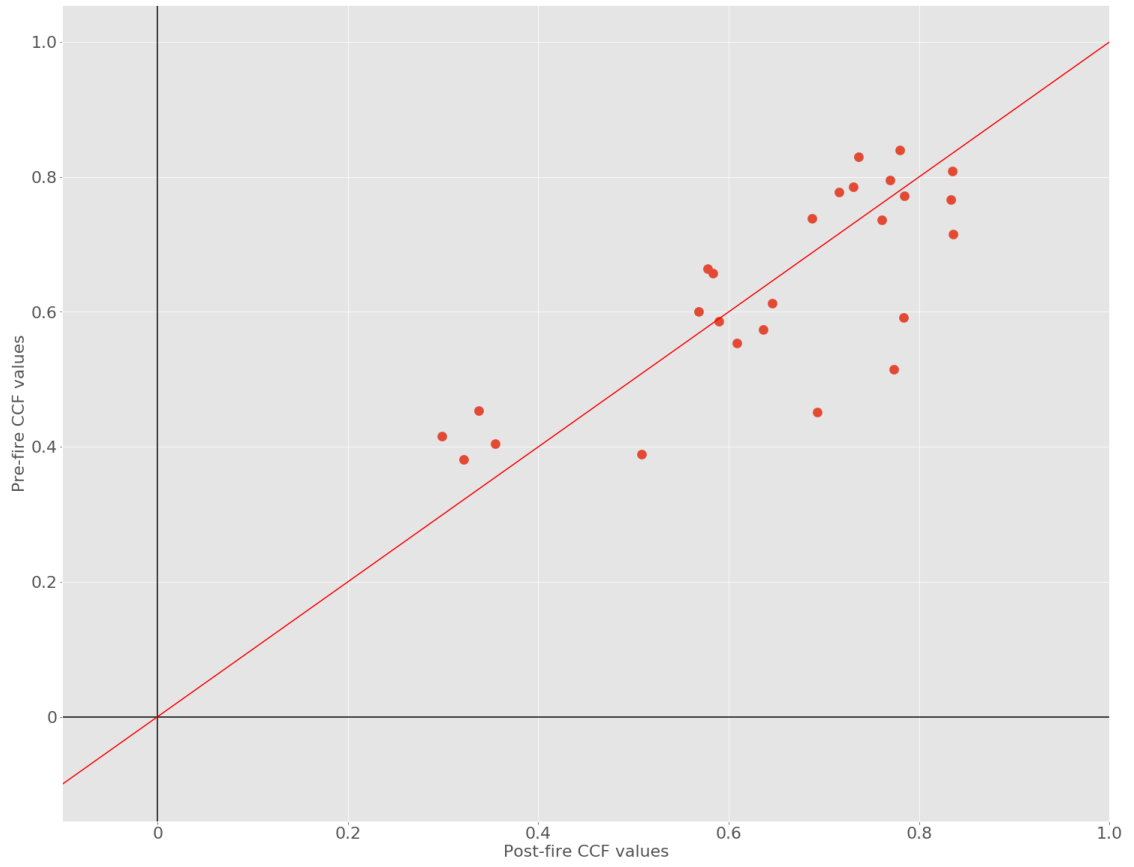


Figure 27 Canopy Cover Fraction (CCF) scatterplot, SA2

REFERENCES

- Assis, T. O., Aguiar, A. P. D. de, Randow, C. von, Gomes, D. M. de P., Kury, J. N., Ometto, J. P. H. B., & Nobre, C. A. (2020). CO₂ emissions from forest degradation in Brazilian Amazon. *Environmental Research Letters*, *15*(10), 104035. <https://doi.org/10.1088/1748-9326/ab9cfc>
- Australian Government Bureau of Meteorology. (n.d.). *Australian Climate Averages—Rainfall*. Retrieved November 16, 2022, from http://www.bom.gov.au/jsp/ncc/climate_averages/rainfall/index.jsp
- Baker, A. G., Catterall, C., Wiseman, M., Baker, A. G., Catterall, C., & Wiseman, M. (2022). Rainforest persistence and recruitment after Australia's 2019–2020 fires in subtropical, temperate, dry and littoral rainforests. *Australian Journal of Botany*, *70*(3), 189–203. <https://doi.org/10.1071/BT21091>
- Barrington Tops National Park, Mount Royal National Park and Barrington Tops State Conservation Area Plan of Management*. (2022). Environment and Heritage Department of Planning and Environment.
- Bergen, K., Goetz, S., Dubayah, R., Henebry, G., Hunsaker, C., Imhoff, M., Nelson, R., Parker, G., Radeloff, V., & Bergen, C. (2009). Remote sensing of vegetation 3-D structure for biodiversity and habitat: Review and implications for lidar and radar spaceborne missions. *Journal of Geophysical Research*, *114*. <https://doi.org/10.1029/2008JG000883>

- Bishop, B. D., Dietterick, B. C., White, R. A., & Mastin, T. B. (2014). Classification of Plot-Level Fire-Caused Tree Mortality in a Redwood Forest Using Digital Orthophotography and LiDAR. *Remote Sensing*, 6(3), Article 3. <https://doi.org/10.3390/rs6031954>
- Boer, M. M., Macfarlane, C., Norris, J., Sadler, R. J., Wallace, J., & Grierson, P. F. (2008). Mapping burned areas and burn severity patterns in SW Australian eucalypt forest using remotely-sensed changes in leaf area index. *Remote Sensing of Environment*, 112(12), 4358–4369. <https://doi.org/10.1016/j.rse.2008.08.005>
- Boer, M. M., Resco de Dios, V., & Bradstock, R. A. (2020). Unprecedented burn area of Australian mega forest fires. *Nature Climate Change*, 10(3), Article 3. <https://doi.org/10.1038/s41558-020-0716-1>
- Boucher, P. B., Hancock, S., Orwig, D. A., Duncanson, L., Armston, J., Tang, H., Krause, K., Cook, B., Paynter, I., Li, Z., Elmes, A., & Schaaf, C. (2020). Detecting Change in Forest Structure with Simulated GEDI Lidar Waveforms: A Case Study of the Hemlock Woolly Adelgid (HWA; *Adelges tsugae*) Infestation. *Remote Sensing*, 12(8), Article 8. <https://doi.org/10.3390/rs12081304>
- Bowman, D. M. J. S., Williamson, G. J., Price, O. F., Ndalila, M. N., & Bradstock, R. A. (2021). Australian forests, megafires and the risk of dwindling carbon stocks. *Plant, Cell & Environment*, 44(2), 347–355. <https://doi.org/10.1111/pce.13916>
- California Government. (2019). *2018 Incident Report Archive*. <https://www.fire.ca.gov/incidents/2018/>
- Camarretta, N., Harrison, P. A., Bailey, T., Potts, B., Lucieer, A., Davidson, N., & Hunt, M. (2020). Monitoring forest structure to guide adaptive management of forest restoration: A

review of remote sensing approaches. *New Forests*, 51(4), 573–596.

<https://doi.org/10.1007/s11056-019-09754-5>

Chen, J. M., Rich, P. M., Gower, S. T., Norman, J. M., & Plummer, S. (1997). Leaf area index of boreal forests: Theory, techniques, and measurements. *Journal of Geophysical Research: Atmospheres*, 102(D24), 29429–29443. <https://doi.org/10.1029/97JD01107>

Chuvieco, E., Martín, M. P., & Palacios, A. (2002). Assessment of different spectral indices in the red-near-infrared spectral domain for burned land discrimination. *International Journal of Remote Sensing*, 23(23), 5103–5110.

<https://doi.org/10.1080/01431160210153129>

Cocke, A. E., Fulé, P. Z., Crouse, J. E., Cocke, A. E., Fulé, P. Z., & Crouse, J. E. (2005).

Comparison of burn severity assessments using Differenced Normalized Burn Ratio and ground data. *International Journal of Wildland Fire*, 14(2), 189–198.

<https://doi.org/10.1071/WF04010>

Commonwealth of Australia, Department of Agriculture, Water and the Environment. (2020).

Gondwana Rainforests of Australia State of Conservation update—April 2020.

Davey, S. M., & Sarre, A. (2020). Editorial: The 2019/20 Black Summer bushfires. *Australian Forestry*, 83(2), 47–51. <https://doi.org/10.1080/00049158.2020.1769899>

De Santis, A., & Chuvieco, E. (2009). GeoCBI: A modified version of the Composite Burn Index for the initial assessment of the short-term burn severity from remotely sensed data. *Remote Sensing of Environment*, 113(3), 554–562.

<https://doi.org/10.1016/j.rse.2008.10.011>

- Dubayah, R., Armston, J., Healey, S. P., Bruening, J. M., Patterson, P. L., Kellner, J. R., Duncanson, L., Saarela, S., Ståhl, G., Yang, Z., Tang, H., Blair, J. B., Fatoyinbo, L., Goetz, S., Hancock, S., Hansen, M., Hofton, M., Hurtt, G., & Luthcke, S. (2022). GEDI launches a new era of biomass inference from space. *Environmental Research Letters*, 17(9), 095001. <https://doi.org/10.1088/1748-9326/ac8694>
- Dubayah, R., Blair, J. B., Goetz, S., Fatoyinbo, L., Hansen, M., Healey, S., Hofton, M., Hurtt, G., Kellner, J., Luthcke, S., Armston, J., Tang, H., Duncanson, L., Hancock, S., Jantz, P., Marselis, S., Patterson, P. L., Qi, W., & Silva, C. (2020). The Global Ecosystem Dynamics Investigation: High-resolution laser ranging of the Earth's forests and topography. *Science of Remote Sensing*, 1, 100002. <https://doi.org/10.1016/j.srs.2020.100002>
- Dubayah, R. O., & Drake, J. B. (2000). Lidar Remote Sensing for Forestry. *Journal of Forestry*, 98(6), 44–46. <https://doi.org/10.1093/jof/98.6.44>
- Dubayah, R.O., Armston, J., Kellner, J.R., Duncanson, L., Healey, S.P., Patterson, P.L., Hancock, S., Tang, H., Hofton, M.A., Blair, J.B., & Luthcke, S.B. (2021). *Global Ecosystem Dynamics Investigation (GEDI) GEDI L4A Footprint Level Aboveground Biomass Density, Version 1* [HDF5]. 0 MB. <https://doi.org/10.3334/ORNLDAAAC/1907>
- Dubayah, R.O., Armston, J., Kellner, J.R., Duncanson, L., Healey, S.P., Patterson, P.L., Hancock, S., Tang, H., Hofton, M.A., Blair, J.B., & Luthcke, S.B. (2022). *Global Ecosystem Dynamics Investigation (GEDI) GEDI L4A Footprint Level Aboveground Biomass Density, Golden Weeks, Version 1* [HDF5]. 0 MB. <https://doi.org/10.3334/ORNLDAAAC/2028>

- Duncanson, L., Kellner, J. R., Armston, J., Dubayah, R., Minor, D. M., Hancock, S., Healey, S. P., Patterson, P. L., Saarela, S., Marselis, S., Silva, C. E., Bruening, J., Goetz, S. J., Tang, H., Hofton, M., Blair, B., Luthcke, S., Fatoyinbo, L., Abernethy, K., ... Zraggen, C. (2022). Aboveground biomass density models for NASA's Global Ecosystem Dynamics Investigation (GEDI) lidar mission. *Remote Sensing of Environment*, 270, 112845. <https://doi.org/10.1016/j.rse.2021.112845>
- Duncanson, L., Neuenschwander, A., Hancock, S., Thomas, N., Fatoyinbo, T., Simard, M., Silva, C. A., Armston, J., Luthcke, S. B., Hofton, M., Kellner, J. R., & Dubayah, R. (2020). Biomass estimation from simulated GEDI, ICESat-2 and NISAR across environmental gradients in Sonoma County, California. *Remote Sensing of Environment*, 242, 111779. <https://doi.org/10.1016/j.rse.2020.111779>
- Fassnacht, F. E., Schmidt-Riese, E., Kattenborn, T., & Hernández, J. (2021). Explaining Sentinel 2-based dNBR and RdNBR variability with reference data from the bird's eye (UAS) perspective. *International Journal of Applied Earth Observation and Geoinformation*, 95, 102262. <https://doi.org/10.1016/j.jag.2020.102262>
- Fisher, D., Lopez, M. J., Davidson, E., & Butt, N. (2021). *Survival and recovery of threatened animal species in fire-affected Gondwana Rainforest World Heritage Areas*. National Environmental Science Programme.
- Fouladinejad, F., Matkan, A., Hajeb, M., & Brakhasi, F. (2019). History and Applications of Space-Borne Lidars. *ISPRS - International Archives of the Photogrammetry, Remote Sensing and Spatial Information Sciences*, 4218, 407–414. <https://doi.org/10.5194/isprs-archives-XLII-4-W18-407-2019>

- Franco, M. G., Mundo, I. A., & Veblen, T. T. (2020). Field-Validated Burn-Severity Mapping in North Patagonian Forests. *Remote Sensing*, *12*(2), Article 2.
<https://doi.org/10.3390/rs12020214>
- Furlaud, J. M., Prior, L. D., Williamson, G. J., & Bowman, D. M. J. S. (2021). Bioclimatic drivers of fire severity across the Australian geographical range of giant Eucalyptus forests. *Journal of Ecology*, *109*(6), 2514–2536. <https://doi.org/10.1111/1365-2745.13663>
- Gao, Y., Skutsch, M., Paneque-Gálvez, J., & Ghilardi, A. (2020). Remote sensing of forest degradation: A review. *Environmental Research Letters*, *15*(10), 103001.
<https://doi.org/10.1088/1748-9326/abaad7>
- Garnaut, R. (2008). *The Garnaut Climate Change Review*.
- Geary, W. L., Buchan, A., Allen, T., Attard, D., Bruce, M. J., Collins, L., Ecker, T. E., Fairman, T. A., Hollings, T., Loeffler, E., Muscatello, A., Parkes, D., Thomson, J., White, M., & Kelly, E. (2021). Responding to the biodiversity impacts of a megafire: A case study from south-eastern Australia's Black Summer. *Diversity and Distributions*, *n/a*(n/a). <https://doi.org/10.1111/ddi.13292>
- Gelabert, P. J., Montealegre, A. L., Lamelas, M. T., & Domingo, D. (2020). Forest structural diversity characterization in Mediterranean landscapes affected by fires using Airborne Laser Scanning data. *GIScience & Remote Sensing*, *57*(4), 497–509.
<https://doi.org/10.1080/15481603.2020.1738060>
- Giglio, L., Boschetti, L., Roy, D., Hoffmann, A. A., Humber, M., & Hall, J. V. (2020). *Collection 6 MODIS Burned Area Product User's Guide Version 1.3*. 34.

GISGeography. (2021a, June). *Landsat 8 Bands and Band Combinations*. GIS Geography.

<https://gisgeography.com/landsat-8-bands-combinations/>

GISGeography. (2021b, October 29). *Sentinel 2 Bands and Combinations*. GIS Geography.

<https://gisgeography.com/sentinel-2-bands-combinations/>

Griebel, A., Bennett, L., Culvenor, D., Newnham, G., & Arndt, S. (2015). Reliability and limitations of a novel terrestrial laser scanner for daily monitoring of forest canopy dynamics. *Remote Sensing of Environment*, 166.

<https://doi.org/10.1016/j.rse.2015.06.014>

Hall, F. G., Bergen, K., Blair, J. B., Dubayah, R., Houghton, R., Hurtt, G., Kellndorfer, J., Lefsky, M., Ranson, J., Saatchi, S., Shugart, H. H., & Wickland, D. (2011).

Characterizing 3D vegetation structure from space: Mission requirements. *Remote*

Sensing of Environment, 115(11), 2753–2775. <https://doi.org/10.1016/j.rse.2011.01.024>

Hancock, S., Armston, J., Hofton, M., Sun, X., Tang, H., Duncanson, L. I., Kellner, J. R., & Dubayah, R. (2019). The GEDI Simulator: A Large-Footprint Waveform Lidar Simulator for Calibration and Validation of Spaceborne Missions. *Earth and Space Science*, 6(2), 294–310. <https://doi.org/10.1029/2018EA000506>

Hofton, M., & Blair, J. B. (2019). *Algorithm Theoretical Basis Document (ATBD) for GEDI Transmit and Receive Waveform Processing for L1 and L2 Products*. 44.

Hu, T., Ma, Q., Su, Y., Battles, J. J., Collins, B. M., Stephens, S. L., Kelly, M., & Guo, Q. (2019). A simple and integrated approach for fire severity assessment using bi-temporal airborne LiDAR data. *International Journal of Applied Earth Observation and Geoinformation*, 78, 25–38. <https://doi.org/10.1016/j.jag.2019.01.007>

Huang, S., Tang, L., Hupy, J. P., Wang, Y., & Shao, G. (2021). A commentary review on the use of normalized difference vegetation index (NDVI) in the era of popular remote sensing. *Journal of Forestry Research*, 32(1), 1–6. <https://doi.org/10.1007/s11676-020-01155-1>

Hudak, A. T., Morgan, P., Bobbitt, M. J., Smith, A. M. S., Lewis, S. A., Lentile, L. B., Robichaud, P. R., Clark, J. T., & McKinley, R. A. (2007). The Relationship of Multispectral Satellite Imagery to Immediate Fire Effects. *Fire Ecology*, 3(1), 64–90. <https://doi.org/10.4996/fireecology.0301064>

Jolly, M., Cochrane, M., Freeborn, P., Holden, Z., Brown, T., Williamson, G., & Bowman, D. (2015). Climate-induced variations in global wildfire danger from 1979 to 2013. *Nature Communications*. <https://www.nature.com/articles/ncomms8537>

Jones, M., Smith, A., Betts, R., Canadell, J., Prentice, I. C., & Le Quere, C. (2020). *Climate Change Increases the Risk of Wildfires*. Science Brief. <https://sciencebrief.org/briefs/wildfires>

Kane, V. R., North, M. P., Lutz, J. A., Churchill, D. J., Roberts, S. L., Smith, D. F., McGaughey, R. J., Kane, J. T., & Brooks, M. L. (2014). Assessing fire effects on forest spatial structure using a fusion of Landsat and airborne LiDAR data in Yosemite National Park. *Remote Sensing of Environment*, 151, 89–101. <https://doi.org/10.1016/j.rse.2013.07.041>

Kaufman, Y. J., Setzer, A., Justice, C., Tucker, C. J., Pereira, M. C., & Fung, I. (1990). Remote Sensing of Biomass Burning in the Tropics. In J. G. Goldammer (Ed.), *Fire in*

- the Tropical Biota: Ecosystem Processes and Global Challenges* (pp. 371–399). Springer. https://doi.org/10.1007/978-3-642-75395-4_16
- Keeley, J. E. (2009). Fire intensity, fire severity and burn severity: A brief review and suggested usage. *International Journal of Wildland Fire*, 18(1), 116–126. <https://doi.org/10.1071/WF07049>
- Keeley, J. E., & Syphard, A. D. (2021). Large California wildfires: 2020 fires in historical context. *Fire Ecology*, 17(1), 22. <https://doi.org/10.1186/s42408-021-00110-7>
- Kellner, J., Armston, J., & Duncanson, L. (2022). *Algorithm theoretical basis document for GEDI footprint aboveground biomass density*. <https://eartharxiv.org/repository/view/3514/>
- Kemter, M., Fischer, M., Luna, L. V., Schönfeldt, E., Vogel, J., Banerjee, A., Korup, O., & Thonicke, K. (2021). Cascading Hazards in the Aftermath of Australia’s 2019/2020 Black Summer Wildfires. *Earth’s Future*, 9(3), e2020EF001884. <https://doi.org/10.1029/2020EF001884>
- Kirillina, K., Shvetsov, E. G., Protopopova, V. V., Thiesmeyer, L., & Yan, W. (2020). Consideration of anthropogenic factors in boreal forest fire regime changes during rapid socio-economic development: Case study of forestry districts with increasing burnt area in the Sakha Republic, Russia. *Environmental Research Letters*, 15(3), 035009. <https://doi.org/10.1088/1748-9326/ab6c6e>
- Kolden, C. A., Smith, A. M. S., Abatzoglou, J. T., Kolden, C. A., Smith, A. M. S., & Abatzoglou, J. T. (2015). Limitations and utilisation of Monitoring Trends in Burn

- Severity products for assessing wildfire severity in the USA. *International Journal of Wildland Fire*, 24(7), 1023–1028. <https://doi.org/10.1071/WF15082>
- Kooyman, R. M., Watson, J., & Wilf, P. (2020). Protect Australia’s Gondwana Rainforests. *Science*, 367(6482), 1083–1083. <https://doi.org/10.1126/science.abb2046>
- Laidlaw, M. J., Hines, H. B., Melzer, R. I., & Churchill, T. B. (2022). Beyond bushfire severity: Mapping the ecological impact of bushfires on the Gondwana Rainforests of Australia World Heritage Area. *Australian Zoologist*, 42(2), 502–513. <https://doi.org/10.7882/AZ.2022.027>
- Law, B. S., Madani, G., Lloyd, A., Gonsalves, L., Hall, L., Sujaraj, A., Brassil, T., & Turbill, C. (2022). Australia’s 2019–20 mega-fires are associated with lower occupancy of a rainforest-dependent bat. *Animal Conservation*, n/a(n/a). <https://doi.org/10.1111/acv.12805>
- Lee, J. S., Cornwell, W. K., & Kingsford, R. T. (2022). Rainforest bird communities threatened by extreme fire. *Global Ecology and Conservation*, 33, e01985. <https://doi.org/10.1016/j.gecco.2021.e01985>
- Lentile, L. B., Smith, A. M. S., Hudak, A. T., Morgan, P., Bobbitt, M. J., Lewis, S. A., Robichaud, P. R., Lentile, L. B., Smith, A. M. S., Hudak, A. T., Morgan, P., Bobbitt, M. J., Lewis, S. A., & Robichaud, P. R. (2009). Remote sensing for prediction of 1-year post-fire ecosystem condition. *International Journal of Wildland Fire*, 18(5), 594–608. <https://doi.org/10.1071/WF07091>

- Liu, A., Cheng, X., & Chen, Z. (2021). Performance evaluation of GEDI and ICESat-2 laser altimeter data for terrain and canopy height retrievals. *Remote Sensing of Environment*, 264, 112571. <https://doi.org/10.1016/j.rse.2021.112571>
- Magnussen, S., & Wulder, M. A. (2012). Post-Fire Canopy Height Recovery in Canada's Boreal Forests Using Airborne Laser Scanner (ALS). *Remote Sensing*, 4(6), Article 6. <https://doi.org/10.3390/rs4061600>
- Miller, J. D., & Thode, A. E. (2007). Quantifying burn severity in a heterogeneous landscape with a relative version of the delta Normalized Burn Ratio (dNBR). *Remote Sensing of Environment*, 109(1), 66–80. <https://doi.org/10.1016/j.rse.2006.12.006>
- Montealegre, A. L., Lamelas, M. T., Tanase, M. A., & De la Riva, J. (2014). Forest Fire Severity Assessment Using ALS Data in a Mediterranean Environment. *Remote Sensing*, 6(5), Article 5. <https://doi.org/10.3390/rs6054240>
- New WWF report: 3 billion animals impacted by Australia's bushfire crisis.* (2020, July 28). <https://www.wwf.org.au/news/news/2020/3-billion-animals-impacted-by-australia-bushfire-crisis>
- Ni, W., Zhang, Z., & Sun, G. (2021). Assessment of Slope-Adaptive Metrics of GEDI Waveforms for Estimations of Forest Aboveground Biomass over Mountainous Areas. *Journal of Remote Sensing*, 2021. <https://doi.org/10.34133/2021/9805364>
- Ni-Meister, W., Jupp, D. L. B., & Dubayah, R. (2001). *Modeling lidar waveforms in heterogeneous and discrete canopies.* <https://doi.org/10.1109/36.951085>
- Nolan, R. H., Boer, M. M., Collins, L., Resco de Dios, V., Clarke, H., Jenkins, M., Kenny, B., & Bradstock, R. A. (2020). Causes and consequences of eastern Australia's 2019–20

season of mega-fires. *Global Change Biology*, 26(3), 1039–1041.

<https://doi.org/10.1111/gcb.14987>

Office of Environment & Heritage. (2011). *Plan of Management Willi Willi National Park*.

NSW National Parks & Wildlife Service. [chrome-](#)

<extension://efaidnbmnnnibpcajpcgiclfndmkaj/https://www.environment.nsw.gov.au/->

</media/OEH/Corporate-Site/Documents/Parks-reserves-and-protected-areas/Parks-plans->

<of-management/willi-willi-national-park-plan-of-management-110822.pdf>

Patterson, P. L., Healey, S. P., Ståhl, G., Saarela, S., Holm, S., Andersen, H.-E., Dubayah, R.

O., Duncanson, L., Hancock, S., Armston, J., Kellner, J. R., Cohen, W. B., & Yang, Z.

(2019). Statistical properties of hybrid estimators proposed for GEDI—NASA’s global ecosystem dynamics investigation. *Environmental Research Letters*, 14(6), 065007.

<https://doi.org/10.1088/1748-9326/ab18df>

Potapov, P., Li, X., Hernandez-Serna, A., Tyukavina, A., Hansen, M. C., Kommareddy, A.,

Pickens, A., Turubanova, S., Tang, H., Silva, C. E., Armston, J., Dubayah, R., Blair, J.

B., & Hofton, M. (2021). Mapping global forest canopy height through integration of

GEDI and Landsat data. *Remote Sensing of Environment*, 253, 112165.

<https://doi.org/10.1016/j.rse.2020.112165>

Quirós, E., Polo, M.-E., & Fragoso-Campón, L. (2021). GEDI Elevation Accuracy

Assessment: A Case Study of Southwest Spain. *IEEE Journal of Selected Topics in*

Applied Earth Observations and Remote Sensing, 14, 5285–5299.

<https://doi.org/10.1109/JSTARS.2021.3080711>

- Reilly, S., Clark, M. L., Bentley, L. P., Matley, C., Piazza, E., & Oliveras Menor, I. (2021). The Potential of Multispectral Imagery and 3D Point Clouds from Unoccupied Aerial Systems (UAS) for Monitoring Forest Structure and the Impacts of Wildfire in Mediterranean-Climate Forests. *Remote Sensing*, *13*(19), Article 19. <https://doi.org/10.3390/rs13193810>
- Rishmawi, K., Huang, C., & Zhan, X. (2021). Monitoring Key Forest Structure Attributes across the Conterminous United States by Integrating GEDI LiDAR Measurements and VIIRS Data. *Remote Sensing*, *13*(3), Article 3. <https://doi.org/10.3390/rs13030442>
- Roy, D. P., Boschetti, L., & Trigg, S. N. (2006). Remote sensing of fire severity: Assessing the performance of the normalized burn ratio. *IEEE Geoscience and Remote Sensing Letters*, *3*(1), 112–116. <https://doi.org/10.1109/LGRS.2005.858485>
- Saunders, M. E., Barton, P. S., Bickerstaff, J. R. M., Frost, L., Latty, T., Lessard, B. D., Lowe, E. C., Rodriguez, J., White, T. E., & Umbers, K. D. L. (2021). Limited understanding of bushfire impacts on Australian invertebrates. *Insect Conservation and Diversity*, *14*(3), 285–293. <https://doi.org/10.1111/icad.12493>
- Scarth, P., Armston, J., Lucas, R., & Bunting, P. (2019). A Structural Classification of Australian Vegetation Using ICESat/GLAS, ALOS PALSAR, and Landsat Sensor Data. *Remote Sensing*, *11*(2), Article 2. <https://doi.org/10.3390/rs11020147>
- Scott Morrison. (2020, February 20). *National Royal Commission into Black Summer bushfires established*. Prime Minister of Australia. <https://www.pm.gov.au/media/national-royal-commission-black-summer-bushfires-established>

- Shiraishi, T., & Hirata, R. (2021). Estimation of carbon dioxide emissions from the megafires of Australia in 2019–2020. *Scientific Reports*, *11*(1), 8267.
<https://doi.org/10.1038/s41598-021-87721-x>
- Tang, H., & Armston, J. (2019). *Algorithm Theoretical Basis Document (ATBD) for GEDI L2B Footprint Canopy Cover and Vertical Profile Metrics*. 39.
- Tang, H., Dubayah, R., Swatantran, A., Hofton, M., Sheldon, S., Clark, D. B., & Blair, B. (2012). Retrieval of vertical LAI profiles over tropical rain forests using waveform lidar at La Selva, Costa Rica. *Remote Sensing of Environment*, *124*, 242–250.
<https://doi.org/10.1016/j.rse.2012.05.005>
- Toth, C., & Józków, G. (2016). Remote sensing platforms and sensors: A survey. *ISPRS Journal of Photogrammetry and Remote Sensing*, *115*, 22–36.
<https://doi.org/10.1016/j.isprsjprs.2015.10.004>
- Tran, B. N., Tanase, M. A., Bennett, L. T., & Aponte, C. (2018). Evaluation of Spectral Indices for Assessing Fire Severity in Australian Temperate Forests. *Remote Sensing*, *10*(11), Article 11. <https://doi.org/10.3390/rs10111680>
- U.S. Geological Survey. (n.d.). *Landsat Normalized Burn Ratio*. Retrieved January 12, 2022, from <https://www.usgs.gov/landsat-missions/landsat-normalized-burn-ratio>
- van Gerrevink, M. J., & Veraverbeke, S. (2021). Evaluating the Hyperspectral Sensitivity of the Differenced Normalized Burn Ratio for Assessing Fire Severity. *Remote Sensing*, *13*(22), Article 22. <https://doi.org/10.3390/rs13224611>
- van Oldenborgh, G. J., Krikken, F., Lewis, S., Leach, N. J., Lehner, F., Saunders, K. R., van Weele, M., Haustein, K., Li, S., Wallom, D., Sparrow, S., Arrighi, J., Singh, R. K., van

- Aalst, M. K., Philip, S. Y., Vautard, R., & Otto, F. E. L. (2021). Attribution of the Australian bushfire risk to anthropogenic climate change. *Natural Hazards and Earth System Sciences*, 21(3), 941–960. <https://doi.org/10.5194/nhess-21-941-2021>
- Wang, C., Elmore, A. J., Numata, I., Cochrane, M. A., Shaogang, L., Huang, J., Zhao, Y., & Li, Y. (2022). Factors affecting relative height and ground elevation estimations of GEDI among forest types across the conterminous USA. *GIScience & Remote Sensing*, 59(1), 975–999. <https://doi.org/10.1080/15481603.2022.2085354>
- Ward, M., Tulloch, A. I. T., Radford, J. Q., Williams, B. A., Reside, A. E., Macdonald, S. L., Mayfield, H. J., Maron, M., Possingham, H. P., Vine, S. J., O'Connor, J. L., Massingham, E. J., Greenville, A. C., Woinarski, J. C. Z., Garnett, S. T., Lintermans, M., Scheele, B. C., Carwardine, J., Nimmo, D. G., ... Watson, J. E. M. (2020). Impact of 2019–2020 mega-fires on Australian fauna habitat. *Nature Ecology & Evolution*, 4(10), 1321–1326. <https://doi.org/10.1038/s41559-020-1251-1>
- Werrikimbe National Park | Learn more.* (n.d.). NSW National Parks. Retrieved October 19, 2022, from <https://www.nationalparks.nsw.gov.au/visit-a-park/parks/werrikimbe-national-park/learn-more>
- Werrikimbe National Park | Visitor info.* (n.d.). NSW National Parks. Retrieved November 16, 2022, from <https://www.nationalparks.nsw.gov.au/visit-a-park/parks/werrikimbe-national-park/visitor-info>
- White, J. D., Ryan, K. C., Key, C. C., & Running, S. W. (1996). Remote Sensing of Forest Fire Severity and Vegetation Recovery. *International Journal of Wildland Fire*, 6(3), 125–136. <https://doi.org/10.1071/wf9960125>

Willi Willi National Park / Visitor info. (n.d.). NSW National Parks. Retrieved November 16,

2022, from <https://www.nationalparks.nsw.gov.au/visit-a-park/parks/willi-willi-national-park/visitor-info>

Wilson, N., Bradstock, R., & Bedward, M. (2022). Disturbance causes variation in sub-canopy fire weather conditions. *Agricultural and Forest Meteorology*, 323, 109077.

<https://doi.org/10.1016/j.agrformet.2022.109077>

Wooster, M. J., Roberts, G. J., Giglio, L., Roy, D. P., Freeborn, P. H., Boschetti, L., Justice,

C., Ichoku, C., Schroeder, W., Davies, D., Smith, A. M. S., Setzer, A., Csiszar, I.,

Strydom, T., Frost, P., Zhang, T., Xu, W., de Jong, M. C., Johnston, J. M., ... San-

Miguel-Ayanz, J. (2021). Satellite remote sensing of active fires: History and current

status, applications and future requirements. *Remote Sensing of Environment*, 267,

112694. <https://doi.org/10.1016/j.rse.2021.112694>

Yu, P., Davis, S. M., Toon, O. B., Portmann, R. W., Bardeen, C. G., Barnes, J. E., Telg, H.,

Maloney, C., & Rosenlof, K. H. (2021). Persistent Stratospheric Warming Due to 2019–

2020 Australian Wildfire Smoke. *Geophysical Research Letters*, 48(7).

<https://doi.org/10.1029/2021GL092609>

BIOGRAPHY

Colin G. Flynn received his Associate of Arts in Social Science with a specialization in GIS from Northern Virginia Community College in 2017, then went on to George Mason University to receive his Bachelor of Science in Geography with a minor in GIS. Colin was recognized as the Geography and Geoinformation Science Department's undergraduate student of the year in 2019. Colin works in the private sector as a Geospatial Data Scientist.